Acta Biomaterialia 140 (2022) 530–546

Contents lists available at ScienceDirect

Acta Biomaterialia

journal homepage: www.elsevier.com/locate/actbio

Full length article

Encapsulation of doxorubicin prodrug in heat-triggered liposomes overcomes off-target activation for advanced prostate cancer therapy

Sara Pereira[a,1], Guanglong Ma[a], Li Na[a], Samo Hudoklin[b], Mateja E. Kreft[b], Nina Kostevsek[c], Wafa T. Al-Jamal[a,*]

[a] School of Pharmacy, Queen's University Belfast, United Kingdom
[b] University of Ljubljana, Faculty of Medicine, Institute of Cell Biology, Ljubljana, Slovenia
[c] Department for Nanostructured Materials, Jozef Stefan Institute, Ljubljana, Slovenia

ARTICLE INFO

Article history:
Received 29 August 2021
Revised 14 December 2021
Accepted 17 December 2021
Available online 24 December 2021

Keywords:
Prostate cancer
Prostate-specific antigen (PSA)
Doxorubicin prodrug
Hyperthermia
Low temperature-sensitive liposomes
Targeted therapy
Cardiotoxicity

ABSTRACT

L-377,202 prodrug consists of doxorubicin (Dox) conjugated to a prostate-specific antigen (PSA) peptide substrate that can be cleaved by enzymatically active PSA at the tumor site. Despite the initial promise in phase I trial, further testing of L-377,202 (herein called Dox-PSA) was ceased due to some degree of non-specific activation and toxicity concerns. To improve safety of Dox-PSA, we encapsulated it into low temperature-sensitive liposomes (LTSL) to bypass systemic activation, while maintaining its biological activity upon controlled release in response to mild hyperthermia (HT). A time-dependent accumulation of activated prodrug in the nuclei of PSA-expressing cells exposed to mild HT was observed, showing that Dox-PSA was efficiently released from the LTSL, cleaved by PSA and entering the cell nucleus as free Dox. Furthermore, we have shown that Dox-PSA loading in LTSL can block its biological activity at 37°C, while the combination with mild HT resulted in augmented cytotoxicity in both 2D and 3D PC models compared to the free Dox-PSA. More importantly, Dox-PSA encapsulation in LTSL prolonged its blood circulation and reduced Dox accumulation in the heart of C4-2B tumor-bearing mice over the free Dox-PSA, thus significantly improving Dox-PSA therapeutic window. Finally, Dox-PSA-loaded LTSL combined with HT significantly delayed tumor growth at a similar rate as mice treated with free Dox-PSA in both solid and metastatic PC tumor models. This indicates this strategy could block the systemic cleavage of Dox-PSA without reducing its efficacy *in vivo*, which could represent a safer option to treat patients with locally advanced PC.

Statement of significance

This study investigates a new tactic to tackle non-specific cleavage of doxorubicin PSA-activatable prodrug (L-377,202) to treat advanced prostate cancer. In the present study, we report a nanoparticle-based approach to overcome the non-specific activation of L-377,202 in the systemic circulation. This includes encapsulating Dox-PSA in low temperature-sensitive liposomes to prevent its premature hydrolysis and non-specific cleavage. This class of liposomes offers payload protection against degradation in plasma, improved pharmacokinetics and tumor targeting, and an efficient and controlled drug release triggered by mild hyperthermia (HT) (~42°C). We believe that this strategy holds great promise in bypassing any systemic toxicity concerns that could arise from the premature activation of the prodrug whilst simultaneously being able to control the spatiotemporal context of Dox-PSA cleavage and metabolism.

1. Introduction

At present, prostate cancer (PC) is second-leading cancer in men and the fifth cause of mortality in the male population worldwide [1]. Depending on the risk level, treatment options for men diagnosed with localized PC include active surveillance, prostatectomy,

* Corresponding author at: School of Pharmacy, Queen's University Belfast, Belfast, BT9 7BL, United Kingdom.
E-mail address: w.al-jamal@qub.ac.uk (W.T. Al-Jamal).
[1] Present Addresses: AstraZeneca, Advanced Drug Delivery Group, Pharmaceutical Sciences, Aaron Klug Building, Granta Park, Cambridge CB21 6GH, UK.

https://doi.org/10.1016/j.actbio.2021.12.019

radiation therapy, and/or androgen deprivation therapy (ADT) [2]. However, despite the initial favorable clinical responses to ADT in patients with hormone-sensitive PC, androgen ablation is rarely curative and consequently, virtually all cancers will become unresponsive to ADT and progress to castration-resistant PC (CRPC) within 2 to 3 years [3,4]. Currently, there are several treatment options for men with metastatic CRPC (mCRPC) which have already been approved by FDA or are under revision process, including chemotherapeutics; second-generation hormonal therapy, radiopharmaceutical agents, targeted therapies (poly(ADP-Ribose), polymerase Inhibitors (PARP inhibitors), and immunotherapy [5,6]. Despite the plethora of newly approved drugs, patients diagnosed with mCRPC continue to develop resistance to treatment, leading to poor prognosis and low overall survival [6–9]. Therefore, the emergence of more effective therapies at all disease stages, which can be tailored to prevent drug resistance and ultimately delay progression to genomically complex stages, is still an unmet clinical need. Bypassing chemoresistance and dose-limiting systemic toxicity has urged the development of alternative therapeutic modalities such as prodrugs [10].

Enzyme-cleavable prodrugs have been widely explored in targeted prodrug design [11]. Prostate-specific antigen (PSA) is an attractive target for PC therapy due to its prostate selective expression and involvement in tumor development, metastasis, and angiogenesis [12]. There are a few prodrugs that have been developed for site-directed activation by PSA in the tumor microenvironment. PRX302 (Sophiris Bio Inc.,) is the most clinically advanced PSA-activatable prodrug [13]. This prodrug has been evaluated in Phase II trials and shown to be well-tolerated in patients with clinically significant localized PC [14,15].

Similarly, Merck Research Laboratories have developed the first reported PSA-cleavable prodrug (L-377,202), which resulted from the conjugation of the PSA substrate Glutaryl-Hyp-Ala-Ser-Chg-Gln to the aminoglycoside portion of doxorubicin (Dox) via a Ser-Leu linker [16], which is activated in the tumour into cytotoxic Dox [16]. Despite having reached the clinical setting, this prodrug did not advance beyond Phase I trials due to toxicity concerns [17,18]. In line with this, in preclinical studies with mice, rats, dogs, and monkeys, the intravenous fraction of L-377,202 metabolized to Dox ranged between 28-41% [17]. In efforts to improve the specificity and plasma stability of L-377,202 prodrug, Aloysius and Hu recently coupled a modified peptide sequence (GABA←mGly-Ala-Ser-Chg-Gln) to Dox using a self-immolative 3-aminooxypropionate linker to reduce non-PSA-mediated hydrolysis by human neprilysin [19,20].

In the present study, we propose a nanomedicine-based approach to overcome the non-specific activation of L-377,202 (hereafter named Dox-PSA). This includes encapsulating Dox-PSA in low temperature-sensitive liposomes (LTSL) which work as a shield to prevent its premature hydrolysis and non-specific cleavage. The LTSL used in the present manuscript have a similar composition to the LTSL in ThermoDox® formulation, where the ratio of each lipid component is optimized to prevent drug leakage at body temperature (37°C), while allowing an ultrafast drug release at mild hyperthermic temperature (~42°C). These LTSL contain 10 mol% of a lysolipid lipid (MSPC) responsible for stabilizing pores in the lipid bilayer which greatly enhances its permeability as it undergoes gel-to-liquid phase transition, resulting in burst drug release at temperatures 39-42°C [21,22]. We believe that this strategy holds great promise in terms of bypassing any systemic toxicity concerns that could arise from the premature activation of the prodrug, whilst simultaneously being able to control the spatiotemporal context of Dox-PSA cleavage and metabolism. Additionally, mild HT has shown to synergize with chemotherapy through several mechanisms [23–25] and to increase vascular perfusion and oxygen levels within the tumor [26,27], which could contribute to increasing Dox-PSA therapeutic efficacy.

Herein, we studied the effect of mild HT on the PSA levels and viability of PC cells. Moreover, Dox-PSA selectivity and PSA-mediated hydrolysis were investigated. In efforts to uncover the mechanisms behind Dox-PSA selectivity, trafficking experiments were carried out in PC cells using confocal microscopy and supported by drug-DNA binding studies. Furthermore, Dox-PSA-loaded LTSL were prepared and characterized in terms of size, encapsulation efficiency, and Dox-PSA release. Toxicity studies of Dox-PSA-loaded LTSL in combination with mild HT were performed in C4-2B monolayers and spheroids. Moreover, *in vivo* studies were carried out to evaluate Dox-PSA-loaded LTSL pharmacokinetics and safety profile. Finally, the therapeutic efficacy of this sequentially-activated nanomedicine was evaluated in both solid and metastatic C4-2B tumor-bearing mice.

2. Experimental section

2.1. Materials

PSA-cleavable peptide (MeO_2C-C-$(CH_2)_3$-CO-4-Hyp-Ala-Ser-Chg-Gln-Ser-Leu-OH) was purchased from Cellmano (China). Mu-His-Ser-Ser-Lys-Leu-Gln-AMC, ≥ 99.5% (AMC-PSA), (1-[Bis(dimethylamino)methylene]-1H-1,2,3-triazolo[4,5-b]-pyridinium 3-oxid hexafluorophosphate (HATU), N,N-diisopropylethylamine (DIPEA), doxorubicin hydrochloride (Dox), acetonitrile and N,N-Dimethylformamide, anhydrous 99.8% (DMF), cholesterol (Chol), chloroform ≥ 99.8%, acetonitrile ≥ 99.9%, methanol ≥ 99.9%, sodium chloride ≥ 99.0%, ammonium sulphate ($(NH_4)_2SO_4$), poly-D-lysine (PDL) and resazurin reagent were all purchased from Sigma-Aldrich (UK). Prostate Specific Antigen, enzymatically active from human seminal fluid (PSA) was obtained by Merck (UK). 1,2-dipalmitoyl-sn-glycero-3-phosphocholine (16:0 PC, DPPC) and 1,2-distearoyl-sn-glycero-3- phosphoethanolamine-N-[amino(polyethylene glycol)-2000] ($DSPE\text{-}PEG_{2000}$) were a kind gift from Lipoid GmbH (Ludwigshafen, Germany). 1-stearoyl-2-hydroxy-sn-glycero-3-phosphocholine (18:0 Lyso PC, MSPC) was purchased from Avanti Polar Lipids (USA). Advanced Roswell Park Memorial Institute (RPMI) 1640 containing 2 g/L D-glucose, 110 mg/L sodium pyruvate and non-essential amino acids, GlutaMAX™ supplement 200 mM, penicillin-streptomycin solution (10000 units/mL), 0.05% Trypsin/EDTA, Trypan Blue Stain (0.4%, 1:1 v/v) and Dulbecco's PBS (1X) were all obtained from Invitrogen Gibco1 Life Technologies (UK). Heat inactivated newborn fetal bovine serum (FBS) was purchased from First Link (UK).

2.2. Synthesis of $MeO_2C(CH_2)_3CO$-Hyp-Ala-Ser-Chg-Gln-Ser-Leu-Dox (Dox-PSA)

Dox-PSA was synthesized as previously described [28]. Briefly, HATU (0.0368 mmol, 13.99 mg) was added to 5mL DMF solution of the PSA-cleavable peptide $MeO_2C(CH_2)_3CO$-Hyp-Ala-Ser-Chg-Gln-Ser-Leu-OH (Hyp, *trans*-4-hydroxy-L-proline; Chg, L-cyclohexylglycine) (Cellmano, China) (0.0368 mmol, 48.00 mg; MW = 884.55 g/mol). After stirring the solution for 30 min at room temperature (RT), doxorubicin hydrochloride (0.0735 mmol, 42.60 mg; MW = 579.98 g/mol) was added and the pH of the reaction was neutralized with anhydrous DIPEA (80 µL, 0.459 mmol). The reaction proceeded at RT under nitrogen for 18 h whilst covered in foil. After completion, the reaction was concentrated under vacuum to a dark red oil. A sample of the crude product was taken for mass spectrometry (MALDI-TOF) which was performed in an AXIMA Performance mass spectrometer (Shimadzu, UK) to confirm the identity of the compound. The crude product was then

dissolved in 50 mL of a mixture containing 80% of 0.1% w/v ammonium acetate in deionized water) and 20% acetonitrile and stored at -20°C.

2.3. Purification of Dox-PSA

The solution of the crude Dox-PSA was filtered through a 0.22 µm PES membrane followed by purification by preparative RP-HPLC (Gilson) on a C18 4.6 × 150 mm column (Agilent, UK). A mobile phase consisting of eluent A (0.1% w/v ammonium acetate in deionized water) and eluent B (acetonitrile) was applied in a step gradient as follows: 35% B over 2 min, 35-80% B over 4 min, 80% B over 1 min, and 80-35% B over 2 min. 4 mL injection volume and at a flow rate of 20 mL/min was used to elute the product, which was detected by UV detector at 214 nm. Pure fractions from each run were pooled together, acetonitrile was evaporated under vacuum and the purified product was freeze dried. The dried product was then re-dissolved in 0.1% ammonium acetate, aliquoted, and freeze dried again for storage at -80°C. Mass spectrometry (MALDI-TOF) was performed in an AXIMA Performance (Shimadzu, UK) to confirm the identity of the chromatographic peaks. Purity of the product (31 mg, 23% reaction yield) was checked by analytical RP-HPLC (Agilent 1200 series) on an Eclipse XDB C18 4.6 × 150 mm column (Agilent, UK) and determined to be > 98%.

2.4. PSA hydrolysis of Dox-PSA

The procedure used to investigate the hydrolysis of Dox-PSA was like the one used in the case of AMC-PSA (see Supporting Information), with minor modifications. Briefly, Dox-PSA cleavage by PSA was carried out with the optimized kinetic buffer, which was composed of 25 mM Tris pH 7.6/ 100 mM NaCl/ 10 mM $CaCl_2$/ 0.05% Brij™35. An enzyme to substrate molar ratio of 1:100 was used to be consistent with previous hydrolysis studies using Dox-PSA prodrug [16]. A solution of Dox-PSA in kinetic buffer was added to the enzymatically active PSA also in kinetic buffer to a final volume of 1 mL. Final concentrations of Dox-PSA and PSA were 40 µM and 0.4 µM, respectively. Incubations were carried out at RT, 37°C, and 42°C to study the effect of temperature in Dox-PSA hydrolysis. To prevent sample evaporation and light exposure of the Dox-PSA conjugate, incubations were performed in amber vials sealed with parafilm®. At predefined time points up to 24 h, 50 µL aliquots of reaction mixture were transferred to 600 µL of acetonitrile and stored at -20°C until quantification to stop enzymatic activity. RP-HPLC analysis was carried out using a Perkin Elmer Series 200 pump with a LC240 fluorescence detector operating at 30°C. 50 µL of sample in acetonitrile were injected in an Eclipse XDB C18 4.6 × 150 mm column (Agilent, UK) and a gradient elution was performed. The mobile phase consisted of eluent A (0.1% v/v TFA in deionized water) and eluent B (0.1% v/v TFA in acetonitrile) with a gradient of 5-65% B over 20 min, 65-5% B over 0.1 min, and 5% B over 10 min. The flow rate was set at 1 mL/min and the change in Dox-PSA peak area was detected at an excitation and emission wavelengths of 490 nm and 550 nm, respectively. In this case, PSA substrate hydrolysis was determined by following the decrease in Dox-PSA peak area over time rather than following the appearance of free Dox, because Dox-PSA metabolism generates an intermediate product, Dox-Leu, which complicates the analysis. All measurements were performed in duplicates.

2.5. Drug-DNA binding studies

The ability of Dox and Dox-PSA to bind to DNA was measured by spectrophotometry and spectrofluorometry. Binding of Dox to calf thymus DNA (ctDNA) was determined by the quenching of Dox fluorescence when bound to DNA, as described elsewhere [29]. 10 µM of Dox or Dox-PSA were titrated with increasing amounts of ctDNA in the range of 0-200 µM. All samples were prepared in 5 mM Tris-HCl buffer pH 7.2, 50 mM NaCl and incubated at 37°C for 24 h before spectral analysis. Solutions of ctDNA without Dox or Dox-PSA were used as blanks. The UV-visible absorbance spectra of Dox/Dox-PSA were recorded at RT in the range of 380-600 nm using a Cary 60 UV-Vis spectrophotometer (Agilent, UK). The fluorescence spectra of Dox/Dox-PSA in the presence of ctDNA were recorded at RT in the range of 200-700 nm upon excitation at 480 nm by means of a F-2710 spectrofluorometer (Hitachi, UK). Quartz cuvettes of 1 cm path length (Hellma Analytics) were used.

2.6. Formulation of Dox-PSA-loaded LTSL

Phospholipids DPPC:MSPC:DSPE-PEG_{2000} at a molar ratio of 86:10:4 were dissolved in chloroform:methanol (4:1 v/v). Liposomes were prepared by the lipid film hydration method. Briefly, the organic solvents were evaporated under reduced pressure at 60°C for 1 h using a rotary evaporator (BÜCHI, Labortechnik AG), then flushed with N_2 stream to remove traces of organic solvent. The dried lipid film was then hydrated with ammonium sulphate pH 5.4 (240 mM $(NH_4)_2SO_4$) for 30 min at 60°C. The final total lipid concentration was 5 mM. Liposomes were reduced in size by extrusion through 0.8 µm (7 cycles), 0.2 µm (17 cycles) and 0.1 µm (13 cycles) polycarbonate filters using a mini-extruder (Avanti Polar Lipids). Following extrusion, liposomes were flushed with N_2 and left to anneal overnight at RT. Dox-PSA was loaded into LTSL using the pH gradient method by $(NH_4)_2SO_4$, as described elsewhere for anthracyclines [30]. Briefly, the extraliposomal buffer was exchanged with HBS buffer pH 7.4 by passing the liposome solution through a Sephadex™ G-25 PD-10 column (GE Healthcare Life Sciences). Next, liposomes were incubated with Dox-PSA (20:1 lipid:prodrug molar ratio) at 37°C and 100 rpm for 24 h.

2.7. Purification of Dox-PSA-loaded liposomes

Non-entrapped Dox-PSA was removed using a qEV size exclusion column (IZON Science Europe Ltd). Briefly, 500 µL of Dox-PSA-loaded liposomes were loaded in the qEV column and 500 µL fractions were collected. Fractions 6-9 were pooled together as they contained the prodrug-loaded liposomes. Liposome suspension was concentrated to the starting concentration using an Amicon Ultra-4 Centrifugal Filter Unit 100 KDa MWCO (Merck, UK) before being used.

Dox-PSA encapsulation efficiency (EE, %) was obtained by comparing its fluorescence before and after purification, according to Eq. (1):

$$EE\ (\%) = \frac{I(t)\ after\ purification}{I(t)\ before\ purification} \times\ 100 \qquad (1)$$

Where I(t) is the fluorescence intensity of liposome suspension after liposome disruption. 10 µL of liposome suspensions were diluted 10-fold in HBS pH 7.4 to a final volume of 100 µL and lysed with 10 µL of 1% (w/v) Triton™ X-100. The liposomal lysates (100 µL) were then transferred to 96-well black plates and fluorescence intensity was determined at λex = 485 nm and λem = 590 nm using a FLUOstar™ Omega Multimode Plate Reader (BMG Labtech, Germany).

2.8. Characterization of Dox-PSA-loaded LTSL

2.8.1. Dynamic light scattering (DLS)

The mean hydrodynamic diameter (Z-ave) and size distribution (polydispersity index, PdI) of the liposomal suspensions were estimated using DLS, and the zeta potential (ζ-potential) was determined by Laser Doppler electrophoresis using a Malvern Zetasizer Nano ZS90 (Malvern). Fisherbrand™ disposable polystyrene

cuvettes and disposable plain folded capillary Zeta cells (Malvern) were used. Liposomes were diluted 100-fold and 10-fold in 0.2 µm filtered deionized water for size and ZP measurements, respectively. Measurements were carried out at a constant temperature of 25°C. The hydrodynamic size was reported as the average value of three measurements, while the ζ-potential measurements were performed in quintuplicate.

2.8.2. Cryogenic transmission electron microscopy (cryo-TEM)

Samples for cryo-TEM were prepared as previously described [30,31] by pipetting 3 µL of Dox-PSA-loaded or empty LTSL onto a holey carbon coated grid (Quantifoil 3.5/1). The grid was blotted and vitrified in ethane in a Vitrobot (FEI, The Netherlands). Grids were observed in a FEI T20 electron microscope operating at 200 keV with a Gatan model 626 cryo-stage. Images were recorded under low-dose conditions with a slow scan CCD camera.

2.8.3. Freeze-fracture electron microscopy (FF-EM)

Dox-PSA-loaded and empty LTSL were initially cryoprotected by incubation in 30% glycerol in 0.1 M cacodylate buffer for 60 min at 4°C, previously reported [32]. Subsequently, 1.5 µL of the sample was placed on the copper holder and fast-frozen by immersion into Freon, cooled by liquid nitrogen (-196°C). Frozen samples were immediately transferred to freeze-fracture device (BALZERS, BAF200), fractured (knife temperature was -150°C), shadowed with platinum (nominal angle 45°) and further strengthened by carbon (nominal angle 90°). Replicas were transferred to room temperature and cleaned in sodium hypochlorite solution. Cleaned replicas were picked on copper microscopic grids and were examined with transmission electron microscope (Philips, CM100) running at 80 kV.

2.8.4. Differential scanning calorimetry (DSC)

The gel-to-liquid crystalline phase transition temperature (Tm) of empty and Dox-PSA-loaded LTSL was determined by DSC using a Q200 DSC instrument (TA Instruments, USA). 20 µL of a 10 mM suspension of empty or Dox-PSA-loaded LTSL were placed in Tzero hermetic aluminum pans (TA Instruments, USA) and sealed with Tzero hermetic lids (TA Instruments, USA). DSC reference and sample cells were loaded with 20 µL of HBS pH 7.4 (reference buffer) and liposome suspension, respectively. Thermal analysis was performed by equilibrating the samples at 30°C for 2 min and then heating them from 30 to 60°C at a heating rate of 1°C/min. DSC thermograms were analyzed using a TA Universal Analysis (TA Instruments, USA). The Tm was defined as the onset of the melting peak in the DSC thermogram. Although some studies have used the maximum heat capacity (peak maximum) to describe the T_m [21,33] as this is indeed true for lipids with a symmetrical endotherm, many phospholipids (as it is the case of the liposomes used in this study) have asymmetrical DSC endotherms [34] and therefore we considered more accurate to define the T_m as the extrapolated onset temperature of the DSC curve.

2.8.5. Release studies

The release of Dox and Dox-PSA from LTSL was determined at 37°C and 42°C in HBS pH 7.4 over 60 min. At each time point, samples were collected. Dox release experiments were carried out as previously described by our group [30]. For Dox-PSA release experiments, a different approach was used to quantify the relative amount of prodrug release. As Dox-PSA is not quenched inside the LTSL, we were not able to determine the fluorescence of the released prodrug in the presence of liposomes, as it was the case for Dox-loaded LTSL. Therefore, Dox-PSA release was investigated using an indirect approach in which 500 µL samples were taken at each time point and passed through a qEV size exclusion column (IZON Science Europe Ltd). Fractions containing the liposomes (F6- F9) were pooled together and fluorescence intensity was determined at $\lambda ex = 485$ nm and $\lambda em = 590$ nm using a FLUOstar™ Omega Multimode Plate Reader (BMG Labtech, Germany). It was assumed that the fluorescence intensity of these liposomes was an indication of the amount of Dox-PSA that remained encapsulated at each time point. Thus, the relative Dox-PSA release at each time point was determined as the difference between the encapsulated prodrug at time t = 0 h and the encapsulated prodrug at each time point, as given by Eq. (2):

$$Dox - PSA\ release\ (\%) = \frac{I(s)}{I(0)} \times\ 100 \quad (2)$$

Where *I(s)* is the fluorescence intensity of the Dox-PSA-loaded LTSL at different time points and *I(0)* is the fluorescence intensity of the Dox-PSA-loaded LTSL at time t = 0 h.

2.8.6. Mammalian cell culture and maintenance

LNCaP and PC3 cell lines were purchased from American Type Culture Collection. The LNCaP-derived C4-2B cell line was obtained from (MD Anderson Cancer Center, USA). All PC cell line were cultured and maintained in Advanced RPMI 1640 medium supplemented with 2 mM L-glutamine, 2 g/L D-glucose, 110 µg/mL sodium pyruvate, 100 U/mL penicillin, 100 µg/mL streptomycin and 10% (v/v) heat-inactivated fetal bovine serum (FBS) and maintained in a humidified chamber at 37°C and 5% CO_2.

2.8.7. Effect of mild HT on PSA expression

C4-2B cells were seeded in 35 mm CellBIND® culture dishes (1×10^6 cells) in complete cell culture medium. The next day, the dishes were sealed with parafilm® and incubated in a water bath at 42°C for 1 h. After HT exposure, the dishes were placed back in the humidified incubator at 37°C and 5% CO_2 until endpoint analysis. Non-heated cells (37°C) were used as a control of PSA basal expression. Immediately after HT or 6, 24 or 48 h after incubation, cells were washed twice with 1 mL of ice-cold PBS before being lysed for RT-qPCR or Western blotting.

2.8.8. Effect of mild HT on the viability of PC cells

LNCaP (1.5×10^4 cells/well), C4-2B (1×10^4 cells/well), and PC3 (1×10^4 cells/well) cells were seeded in 96-well culture plates in complete medium. The next day, the plates were sealed with parafilm® and incubated in a water bath at 42°C for 1 h. After HT exposure, the plates were placed back in the humidified incubator at 37°C and 5% CO_2 until end point analysis. Non-heated cells (37°C) were used as a positive control of cell viability. After 6, 24 or 48 h of incubation, cell viability was determined using resazurin assay.

2.9. PSA mRNA levels by real-time polymerase chain reaction (RT-qPCR)

2.9.1. RNA extraction from PC cells

For the quantification of PSA mRNA by RT-qPCR, C4-2B and LNCaP (1×10^6 cells) cells were seeded in 35 mm CellBIND® culture dishes in complete culture medium. PC3 (1×10^6 cells) cells were seeded in standard 35 mm culture dishes in complete culture medium. In the experiment to assess the effect of mild HT on PSA expression, mild HT treatment applied for 1 h before RNA extraction. In the experiment to assess the basal PSA levels, RNA was extracted 24 h after cell seeding. Total RNA was isolated from PC cells using PureLink™ RNA Mini Kit (Thermo Scientific™, UK), following manufacturer's instructions. The concentration and purity of the total RNA were determined at 260 nm and 260/280 nm, respectively using a CLARIOstar Multimode microplate reader (BMG Labtech, Germany). The integrity of the RNA was confirmed by visualization on 1% (w/v) agarose gel, which was run at 120 V for

1 h in 1x TAE buffer. DNA-free total RNA was prepared by incubating 1µg (50 µL) of total RNA with 1 U of DNase I for 30 min at 37°C. Following incubation, DNase was inactivated by heating for 10 min at 75°C in the presence of 5 mM of EDTA to prevent RNA hydrolysis.

2.9.2. cDNA synthesis

DNase-free total RNA (1 µg) was reverse transcribed using SuperScript® IV First-Strand cDNA Synthesis Reaction (Thermo Scientific™, UK), according to manufacturer's instructions. An additional step was performed to remove the RNA by incubating the resulting cDNA with 1 µL of *E. coli* RNase H at 37°C for 20 min. The concentration and purity of the cDNA were determined at 260 nm and 260/280 nm, respectively using a CLARIOstar Multimode microplate reader (BMG Labtech, Germany). All samples displayed ratios 260/280 nm between 1.76 and 1.82, indicative of highly pure cDNA.

2.9.3. TaqMan qPCR

Amplification and detection were performed in a Rotor Gene-Q (Qiagen) thermocycler with the following cycling conditions: one step at 50°C for 2 min for Uracil-N-Glycosylase (UNG) incubation, one step at 95°C for 5 min for polymerase activation, and 40 cycles at 95°C for 25 s (denaturation), and 60°C for 1 minute (annealing/extension). For each 20 µL real-time PCR (RT-qPCR) reaction, 1 µL of reverse transcription sample was combined with 8 µL of RNase-free water, 10 µL of TaqMan™ Universal Master Mix II with UNG 2x (Thermo Scientific™, UK) and with 1 µL of TaqMan® Assay 20x. Each PCR run included independent duplicates of each sample and of negative control without template. The TaqMan fluorescent spectra collected during PCR were analysed using the Rotor-Gene 1.7.94 Software (Qiagen, UK). Relative values were obtained from the threshold PCR cycle number (CT, cycle threshold), which is the cycle number at which the sample's fluorescence intersected with the detection threshold and is directly proportional to the amount of DNA in the sample. Relative mRNA levels in each sample were obtained by normalization to its GAPDH content and the comparative CT method was used, as described elsewhere [35]. Briefly, the difference (ΔCT) between the PSA CT values and the GAPDH CT values was determined:

$$\Delta CT = CT\ (PSA) - CT\ (GAPDH) \tag{3}$$

After calculating the value resulting from Eq. (1) for each of the samples, the reference sample was assigned (PC3 cells for basal PSA levels or non-heated cells for effect of mild HT on PSA expression). Next, the difference between each sample's ΔCT and the reference sample ΔCT was determined:

$$\Delta\Delta CT = \Delta CT\ (sample) - \Delta ct\ (reference\ sample) \tag{4}$$

Finally, the results were presented as fold-change, given by $2^{-\Delta\Delta CT}$.

2.9.4. PSA protein expression by Western Blotting (WB)

For the quantification of PSA protein by Western blot (WB), C4-2B and LNCaP (1×10^6 cells) cells were seeded in 35 mm CellBIND® culture dishes in complete culture medium. PC3 (1×10^6 cells) cells were seeded in standard 35 mm culture dishes in complete culture medium. In the experiment to assess the effect of mild HT on PSA expression, mild HT was applied for 1 h before cell lysis. In the experiment to assess the basal PSA levels, cells were lysed 24 h after cell seeding. To prepare the cell lysates for WB, cells were washed twice with 1 mL of ice-cold PBS and lysed with 50 µL/well of RIPA lysis buffer containing protease inhibitors. Cell lysates were incubated on ice for 30 min while vortexing every 10 min. Samples were centrifuged at 16,089 x g for 30 min at 4°C and the supernatants containing proteins were collected. The total protein concentration was determined using Pierce™ BCA Protein Assay Kit (Thermo Scientific™, UK), according to manufacturer's instructions. To prepare samples for SDS-PAGE, 1x loading dye was added to 30 µg of total protein and samples were denatured by heating for 7 min at 95°C. SDS-PAGE was carried out using a Mini-PROTEAN® Tetra Electrophoresis cell (Bio-Rad, UK) in 1x running buffer. Proteins were resolved in 16% (w/v) polyacrylamide separating gel, with a 4% (w/v) stacking gel and run at 100 V for approximately 1.5 h. After SDS-PAGE, proteins were transferred to a Hybond 0.2 µm pore size PVDF membrane using a Mini Trans-Blot® Electrophoretic Transfer Cell (Bio-Rad, UK) in 1x transfer buffer. The electrophoretic transfer was carried out at 70 V for 1.5 h at 4°C. The membrane containing the proteins was blocked with 5% (w/v) non-fat dry milk in TBS-T for 1 h at RT on a shaker. The blot was then incubated with a rabbit anti-PSA monoclonal antibody (Cell Signaling Technology) at a dilution of 1:1,000 in PBS/ 0.025% (v/v) sodium azide overnight at 4°C on a shaker. The blot was then washed three times with 10 mL of TBS-T on a shaker. The blots were then incubated with goat anti-rabbit IgG HRP-conjugate (Cell Signaling Technology) in 1% non-fat dry milk at 1:2,000 dilution for 1 h at RT. Following three washes with TBS-T, the blots were incubated with ECL Western Blotting substrate (GE Healthcare), according to manufacturer's instructions. Protein bands were visualized using a ChemiDoc™ MP Imaging System (Bio-Rad, UK). The intensity of the specific protein bands was quantified using Image Lab™ software (Bio-Rad, UK). β-actin was used as an internal loading control. Thus, after imaging the protein of interest, the blot was washed three times with 10 mL of TBS-T (10 min/wash) on a shaker, followed by incubation with a rabbit β-actin antibody (Cell Signaling Technology) at a dilution of 1:1,000 in PBS/ 0.025% (v/v) sodium azide for 1 h at RT on a shaker. Following three washes with TBS-T, blots were incubated with the same goat anti-rabbit IgG HRP conjugate secondary antibody as mentioned previously in 1% non-fat dry milk at 1:2,000 dilution for 1 h at RT. The same steps of washing after secondary antibody, incubation with chemiluminescent substrate, and protein band visualization were performed as described above. Each immunoblot included independent duplicates of each sample. In the experiments performed to assess the basal PSA levels, the relative PSA expression was determined by normalizing each PSA band to the corresponding β-actin loading control (Eq. (5)). In the experiments performed to assess the effect of mild HT on PSA expression levels, a second normalization was done in respect to the control, non-heated cells (Eq. (6)).

$$Normalized\ PSA = \frac{PSA\ band\ peak\ area}{\beta\ actin\ band\ peak\ area} \tag{5}$$

$$Normalization\ to\ control = \frac{Normalized\ PSA\ of\ sample}{Normalized\ PSA\ of\ control} \tag{6}$$

2.9.5. Internalization studies by confocal laser scanning microscopy

C4-2B cells (6×10^4 cells/well) were seeded onto poly-D-lysine coated 12 mm glass coverslips in 24-well plates, while PC3 cells (6×10^4 cells/well) were seeded onto standard (uncoated) glass coverslips. After 48 h, cells were incubated in complete cell culture media containing 5 µM of free Dox, free Dox-PSA or Dox-PSA-loaded LTSL, according to experiment requirements. In experiments to assess intracellular Dox-PSA release from LTSL, mild HT treatment (42°C for 1 h) was applied immediately after compound addition. Non-heated cells (37°C) were used as a control of cellular uptake. At predefined time points, cells were washed with ice-cold PBS and fixed with 4% (v/v) paraformaldehyde/PBS solution for 15 min at RT. After two additional washing steps with PBS to remove fixative, cells were incubated with 1 µg/mL of Hoechst 33342 for 10 min at RT (in the dark). Following counterstaining, the coverslips were washed once with PBS and mounted onto

glass slides using ProLong™ Gold Antifade mounting media. Images were taken on a Leica SP8 confocal microscope using a 63x oil immersion objective and 405 nm and 488 nm laser detectors in the hybrid (HyD) mode. Images were analyzed usin ImageJ 1.51u (NIH) software.

2.9.6. Endo/lysosomal co-localization studies

C4-2B cells (1.5×10^4 cells/well) were seeded onto poly-D-lysine coated 96-well clear glass bottom plates in complete medium. A higher cell density was used in this experiment compared to that used in cell viability assays performed in the same plate format, because we have observed that C4-2B cells proliferate slower in glass-bottom plates compared to plastic plates. After 48 h, cells were incubated with 1 μM of Dox or 5 μM of Dox-PSA. A lower concentration of Dox was used as in previous cellular uptake experiments, Dox fluorescence intensity was extremely high. Moreover, our aim was not to directly compare Dox with Dox-PSA, but rather to investigate if any of the compounds was internalized by endocytosis and, more importantly, if it can escape the endo/lysosomal compartments. Incubation with drugs was carried out for 3 h in the case of Dox and for 6, 24 or 48 h in the case of Dox- PSA. Again, a lower incubation time was used with Dox due to its faster cellular uptake and the fact that longer incubations would result in high cytotoxicity. At the predetermined time points, cells were washed three times with sterile PBS, followed by the addition of 100 μL LysoTracker® Green DND-26 solution (50 nM) in phenol red-free culture medium. Following incubation with this endo/lysosomal stain for 40 min at 37°C/ 5% CO_2, cells were immediately imaged without fixation. Images were taken by a Leica SP8 confocal microscope using a 40x water objective and 488 nm and 552 nm laser detectors in the hybrid (HyD) mode. Images were analyzed using ImageJ 1.51u (NIH) software.

2.9.7. Viability of PC monolayers measured by resazurin assay

C4-2B cells (1×10^4 cells/well) were seeded onto poly-D-lysine coated 96-well plates in complete medium. PC3 cells (1×10^4 cells/well) were seeded in standard 96-well TC plates in complete medium. After 48 h, a range of concentrations of free Dox, free Dox-PSA, Dox-PSA-loaded LTSL or empty LTSL were prepared in 30 μL of complete medium and added to the cells. Spent medium was not replenished during the time course of the experiment to ensure sufficiently high PSA concentrations. For the experiments with HT, mild HT treatment (42°C) was applied immediately after compound addition. Non-heated cells (37°C) were used as a control. Vehicle-treated cells were used as a 100% viability control. At 24-96 h post-incubation, cell viabilities were determined by resazurin assay [36]. Hence, cells were incubated for 4 h with 0.01 mg/mL resazurin solution in a humidified incubator at 37°C and 5% CO_2. Following incubation, 150 μL of media-containing resazurin were transferred to black 96-well plates and fluorescence intensity was quantified at $\lambda ex = 544$ nm, $\lambda em = 590$ nm using a FLUOstar™ Omega Multimode Plate Reader (BMG Labtech, Germany). The results were presented as the percentage of cell viability (mean ± SEM) and normalized to the vehicle-treated cells or the non-heated cells, depending on the experiment.

2.9.8. Viability of PC spheroids

Spheroids were cultured using the liquid overlay technique, as previously reported [28]. On day 3 post-seeding, 30 μL of medium were removed from each well and a range of concentrations of free Dox-PSA or Dox-PSA-loaded LTSL were prepared in 30 μL of medium and added to the cells. At 48-96 h post-treatment, 100 μL of media were removed and replaced by an equal volume of a 10 mM EDTA disodium salt solution to yield 5 mM final EDTA concentration, as previously reported [28]. Cells were incubated for 30 min at 37°C/ 5% CO_2, followed by addition of resazurin to a final concentration of 0.01 mg/mL. Spheroids were incubated overnight at 37°C/ 5% CO_2 and the next day, 100 μL of media-containing resazurin were transferred to black 96-well plates quantification of fluorescence intensity. EDTA treatment was used as previously described to disrupt the tight junctions on the highly dense C4-2B spheroids, and allow resazurin to penetrate trough the different cells layers of the spheroids. The results were presented as the percentage of cell viability (mean ± SEM) and normalized to the vehicle-treated cells.

2.9.9. Animals and tumor models

NSG mice used in this experiment were bred at Queen's University Belfast (Belfast, UK). All animal procedures were performed according to UK Home Office Code of Practice for the Housing and Care of Animals used in Scientific Procedures. Male NSG mice aged 8 weeks old were placed on Teklad Global 2019X for 5 days prior to both solid and metastatic tumor inoculation. Solid and metastatic C4-2B tumor models were established as previously described by our group [37,38].

Solid tumor model: legs of mice were subcutaneously injected with 25 μL of C4-2B (2.5×10^6 cells) in a serum-free medium with 25 μL high concentration Corning® Matrigel® Matrix, using 27 G needles. Mice had bifocal tumors for imaging, and unifocal tumors for therapy. Tumor growth was monitored three times per week using an electronic caliper, and tumor volumes were calculated using the following equation:

$V=L*W^2/2$ (V stands for tumor volume, L stands for the longest diameter, W stands for the diameter perpendicular to the length).

Metastatic tumor model was established using C4-2B-4 Luc cells which are luciferase-expressing C4-2B-4 cells. These cells are a kind gift from Dr Ning Wang (University of Sheffield, UK). Mice were injected with C4-2B-4-luc cells in PBS (1×10^6 cells) via the tail caudal artery [37]. Sterile luciferin in PBS (15 mg/ mL) were injected subcutaneously in the back of the mice at 10 μL/g of body weight, and the bioluminescence signals were imaged 10-15 min post-injection using In-Vivo Xtreme Imaging System (Bruker Scientific LLC, MA, USA).

2.9.10. Pharmacokinetics of Dox-PSA-loaded LTSL in C4-2B tumor-bearing mice

C4-2B tumor-bearing mice with a tumor size of 600 mm^3 were randomized and grouped into 2 groups (6 mice per group). One group was injected via the tail vein with Dox-PSA (10 mg/kg), and the other group was injected with Dox-PSA-loaded LTSL (equivalent to 10 mg/kg of Dox-PSA). At selected time points, around 100 μL blood was collected, and kept at 4°C overnight, and then centrifuged at 3000 rpm for 5 min to collect serum. To determine the concentration of Dox-PSA (or its metabolites), high performance liquid chromatography (HPLC) was used. Briefly, 30 μL of serum was mixed with 90 μL of cold acetonitrile to precipitate the protein, then the mixture was sonicated for 5 min before centrifugation at 22000 rpm for 10 min. The supernatant was collected for HPLC analysis. HPLC was performed on 1260 Infinity II Fluorescence Detectors (Agilent, US), with a 4.6 × 250 mm, 5 μm Eclipse Plus Phenyl-Hexyl column (Agilent, US) using a water containing 0.1% TFA (A)/acetonitrile (B) mobile phase system and fluorescence detection (ex: 480 nm, em: 585 nm). The gradient was performed at a total flow rate of 1 mL/min, 5-65% B from 0 to 20 min, 65-5% B from 20 to 25 min, 95% B from 25 to 30 min. 24 h post-injection, heart was collected and homogenized using tissuelyser (TissueLyser LT, QIAGEN, Germany) with 400 μL of water containing 0.1% TFA/acetonitrile (1/3, v/v). Then the homogenized tissues were centrifuged at 22000 rpm for 10 min. The supernatant was collected for HPLC analysis as described above. Standard curves for both Dox-PSA and Dox were prepared using HPLC with the same

method described above. For Dox standard curve, Dox HCl was dissolved in water first (5 mg/mL), further diluted to 0.05 mg/mL with PBS. Then it was diluted with acetonitrile to a range of 5000-100 ng/mL. For Dox-PSA standard curve, Dox-PSA was dissolved in 0.1% ammonium acetate/acetonitrile (4/1) first (5 mM), then further diluted with acetonitrile to a range of 10-0.1 µM.

2.9.11. In vivo *release in solid C4-2B tumor model*

C4-2B tumor-bearing mice were shaved to reduce the animal fluorescence background. Mice were injected via the tail vein with 200 µL LTSL-Dox-PSA (10 mg/kg of Dox-PSA). Mice were immediately anaesthetized using inhalational isoflurane, and one tumor bearing leg was immersed in a 42°C water bath for 1 h to trigger drug release. The second tumor-bearing leg was used as a control. Animal body temperature was controlled using a heated pad with a rectal thermocouple. At the end of the treatment, the mice were imaged for Dox-PSA release (excitation filter= 480 nm, emission filter= 600 nm) using In-Vivo Xtreme. 24 h post-injection, mice were sacrificed, and tumors were isolated and imaged. The high background of mice hairy heads was covered in during imaging using a black paper.

2.9.12. Therapy in C4-2B solid tumor model

C4-2B tumor-bearing mice with a tumor size of 50-100 mm^3 were randomized and grouped into 5 groups (5 mice per group). Each group was injected via the tail vein with one of the following treatment; namely PBS (200 µL, +HT), Dox-PSA (10 mg/kg, +HT), Dox-PSA (10 mg/kg, -HT), LTSL-Dox-PSA (10 mg/kg of Dox-PSA, +HT), and LTSL-Dox-PSA (10 mg/kg of Dox-PSA, -HT). Mice were immediately anaesthetized using inhalational isoflurane, and the tumor-bearing leg one was immersed in a 42°C water bath for 1 h. Some groups were not treated with HT. Animal body temperature was controlled using a heated pad with a rectal thermocouple. At the end of the treatment, mice were returned to their cages and observed. The treatment was repeated three times, as indicated in the results section. The body weight and tumor size were monitored three times a week. The tumor growth data were expressed as mean ± SEM (standard error of the mean), with n denoting the number of animals. At the end of the experiment, organs were immediately fixed in 10% neutral buffer formalin. Tissues were then paraffin-embedded and sectioned for haematoxylin and eosin stains (H&E) according to standard histological protocols at the Royal Veterinary College (London, UK).

2.9.13. Therapy in C4-2B-4 bone metastasis model

Two weeks post C4-2B-4-luc cells injection, mice were randomized and grouped into 3 groups (5 mice per group). Each group was injected via the tail vein with one of the following treatments; namely PBS (200 µL, +HT), Dox-PSA (10 mg/kg, +HT), and LTSL-Dox-PSA (10 mg/kg of Dox-PSA, +HT). Mice were immediately anaesthetized using inhalational isoflurane, and both tumor-bearing legs were immersed in a heated water bath for 1 h. Animal body temperature was controlled using a heated pad with a rectal thermocouple. At the end of the treatment, mice were returned to their cages and observed. The treatment was repeated three times, as indicated in the results section. The body weight monitored daily, while tumor growth every 2-3 days. Metastasis growth was monitored using *in vivo* bioluminescence imaging. Mice were injected subcutaneously with sterile luciferin in PBS (15 mg/ mL) at 10 µL/g of body weight. 10-15 min post-injection bioluminescence signals were imaged using In-Vivo Xtreme Imaging System (Bruker Scientific LLC, MA, USA). The tumor growth data were expressed as mean ± SEM (standard error of the mean), with n denoting the number of animals.

2.9.14. Statistical analysis

Data were analyzed by one-way (1 factor, >2 levels) or two-way (2 factors, >2 levels) analysis of variance (ANOVA) with Bonferroni post-hoc tests. Dose-response curves were fitted using a four-parameter logistic nonlinear regression model. Statistical tests and graphs were computed on GraphPad Prism 7.0. Microscopy images were assembled using ImageJ 1.51u (NIH).

3. Results

3.1. Mild HT treatment does not have a detrimental effect on PSA protein levels and PC cell viability

To develop a successful Dox-PSA-loaded LTSL it is crucial to ensure that: 1) PC cell lines expressing high levels of enzymatically active PSA are selected as an *in vitro* model for our mechanistic and cytotoxicity studies; and 2) PSA expression is not downregulated by mild HT temperatures of ~ 42°C, which could otherwise compromise prodrug activation. With this in mind, we started by measuring PSA levels in a range of PC cell lines by Western blot and RT-qPCR. High expression of this serine protease was observed in C4-2B and LNCaP cells, whereas PC3 cells did not show detectable PSA (Fig. 1A & B). In addition, PSA expression was increased in androgen-independent (C4-2B) cells compared to the parental androgen-sensitive (LNCaP) cells, as determined by Western Blot and in agreement with previous studies [28,39]. Interestingly, mRNA levels were similar in both cell lines, which could suggest post-transcriptional modifications occurring in LNCaP mRNA that result in a lower amount of protein, or due to the intrinsically different nature of the techniques. In fact, by Western blot, we analyzed the free form of PSA (34 kDa), whereas RT-qPCR quantified the PSA mRNA pool that will subsequently be translated into a native protein and thus, it is conceivable that despite initially having comparable amounts of PSA mRNA, LNCaP cells have more complexed mRNA compared to C4-2B cells. In good agreement with our results, a former study showed only a moderate increase in PSA mRNA from C4-2B cells compared to LNCaP cells, while a much more pronounced PSA band was obtained by Western blot for C4-2B cell line [40]. Consequently, the higher levels of PSA in C4-2B cells compared to LNCaP cells suggest that C4-2B cell line could potentially constitute a more predictive model to study PSA-cleavable prodrugs for CRPC and the results hereafter will, therefore, focus on this cell line.

As stated earlier, a major constraint to the development of Dox-PSA-loaded LTSL combined with mild HT is that PSA expression must not be downregulated by mild HT (~ 42°C), which could otherwise compromise prodrug activation. With this in mind, we then investigated whether PSA levels were altered by exposing C4-2B cells to mild HT (42°C). A mild HT treatment regimen of 1 h was selected based on our studies (Supporting Fig. S1) and to be clinically feasible (NCT00826085 & NCT02567383). Higher temperature than 43°C was not studied as cell death and thermotolerance was previously reported at higher temperatures [41,42]. Thus, cells were incubated for 1 h at 42°C, and then lysed either immediately (0 h) or at 6, 24, and 48 h post-HT, during which time cells were allowed to recover at 37°C. RT-qPCR results revealed that PSA mRNA levels in C4-2B cells were reduced up to 6 h post-HT treatment; however, not accompanied by a concomitant decrease in protein levels (Fig. 1**C**). Additionally, to evaluate the impact of fever-range HT in PC cell viability, LNCaP, C4-2B, and PC3 cells were exposed to the same heat treatment as the one used in RT-qPCR and WB. LNCaP and C4-2B cell viabilities remained unchanged relative to the untreated controls for all post-HT time points. PC3 cells, however, showed approximately 10-20% reduction in cell viability at 6-24 h post-treatment, but they recovered after incubation at physiological temperature for 48 h (Fig. 1**D**). These results are in

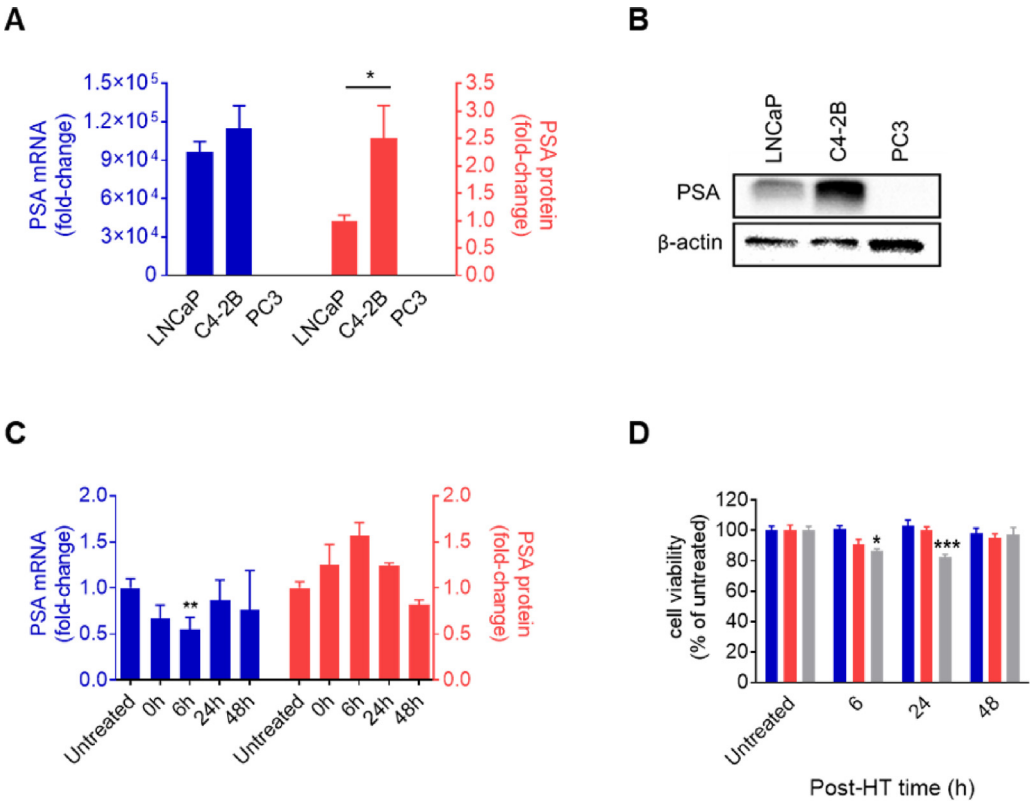

Fig. 1. PSA basal levels in PC cells and effect of mild HT on the PSA expression and viability of C4-2B cells. (A) PSA mRNA (blue bars) and protein levels (red bars) determined by RT-qPCR and Western blot, respectively. Expression levels are shown as fold-change in comparison to PC3 cells that lack PSA. **(B)** Representative blot showing PSA constitutive expression in PC cells. β-actin was used as an internal loading control. The results are representative of two independent experiments. **(C)** PSA mRNA (blue bars) and protein levels (red bars) in C4-2B cells exposed to 1 h of mild HT (42°C) as measured by RT-qPCR and Western blot, respectively**.** Relative mRNA levels were normalized to the respective GAPDH (internal control) of each sample. Results were expressed as fold-change, which is given by $2^{-\Delta\Delta CT}$, where $\Delta\Delta CT = \Delta CT_{\text{target gene}} - \Delta CT_{\text{GAPDH}}$. Data shown as mean ± SD (n = 2). PSA expression levels were quantified by Western blot band densitometry. Each PSA band intensity was normalized by its respective β-actin and the value obtained was subsequently normalized to the untreated (non-heated) cells. Data shown as mean ± SD (n = 2). **(D)** Cell viability of C4-2B (blue bars), LNCaP (red bars) and PC3 (grey bars) cells exposed to 1 h of mild HT (42°C). Cell viability was assessed by resazurin assay after 6, 24 or 48 h post-treatment. Results are expressed as a percentage of untreated (non-heated) cells. Data shown as mean ± SEM (n = 6). Statistical analysis was performed using one-way ANOVA followed by Bonferroni post-hoc test. Statistical significance (* $p < 0.05$, ** $p < 0.01$, *** $p < 0.001$).

good agreement with previous findings that describe 42.5°C as the inflection point of HT, where cancer cells exposed to higher temperatures (> 42.5°C) undergo cell death [43].

3.2. Dox-PSA selectivity for PSA-expressing PC cells

A specific and efficient PSA-mediated hydrolysis is a prerequisite to establish Dox-PSA as a nanomedicine drug. Herein, Dox-PSA was synthesized as previously described [28] and incubated with enzymatically active PSA in the optimized kinetic buffer, as described in Supporting Fig. S2. Interestingly, over 94% of the prodrug was hydrolyzed over 24 h, with no effect of temperature on its hydrolysis (Fig. 2**A**). This finding indicates that mild HT treatment can be used to trigger prodrug release from the LTSL, without compromising Dox-PSA activation by PSA.

Understanding how Dox-PSA is taken up by PC cells and where prodrug activation occurs is essential for the successful development of a Dox-PSA nanomedicine. The literature on PSA-cleavable prodrugs has consistently relied on the extracellular activation of the prodrug. However, our group has previously shown that PSA-mediated hydrolysis of Dox-PSA can also take place inside PSA-expressing cells [28]. This finding is important in the context of our proposed therapeutic approach of combining LTSL-Dox-PSA with mild HT, as the prodrug (or at least fraction of it) would be released and activated intracellularly. Here, C4-2B and PC3 cells were incubated with 5 μM of either free Dox or Dox-PSA, after which confocal laser scanning microscopy (CLSM) was performed. Dox/Dox-PSA intrinsic fluorescence was used to easily track the drug/prodrug inside the cells. No differences in Dox uptake were observed between the two cell lines, where intense fluorescence signals were seen in the nuclei of these cells across all time points tested (Fig. 2**B**). Besides, the high Dox intracellular uptake resulted in weak nuclear staining, as Dox and Hoechst compete for their binding with the nuclei of the cells, as reported elsewhere [44]. Conversely, Dox-PSA fluorescence was localized in the cytosol and perinuclear region of PC3 cells, with no nuclear uptake observed for at least 48 h (Fig. 2**B**). Furthermore, lower fluorescence signals were detected in the cytoplasm at 48 h, suggesting prodrug metabolism or excretion without activation, which requires further investigation. On the other hand, C4-2B cells that were incubated with Dox-PSA for 6 h exhibited punctuated fluorescent signals that were restricted to the cytosol. Interestingly, longer incubation time resulted in Dox-PSA activation in C4-2B cells, as shown by the presence of nuclear fluorescence at 24 h (Fig. 2B & Supporting Fig. S3). These results support Dox selective nuclear uptake in PSA-expressing cells and indicate that Dox-PSA does not enter the nucleus until it is cleaved into free Dox [45], since nuclear uptake was absent in PSA-non-expressing PC3 cells.

Another notable feature of Dox-PSA uptake was the fact that its internalization was much slower compared to Dox. While the parental drug was observed in the nuclei of the cells after 30 min

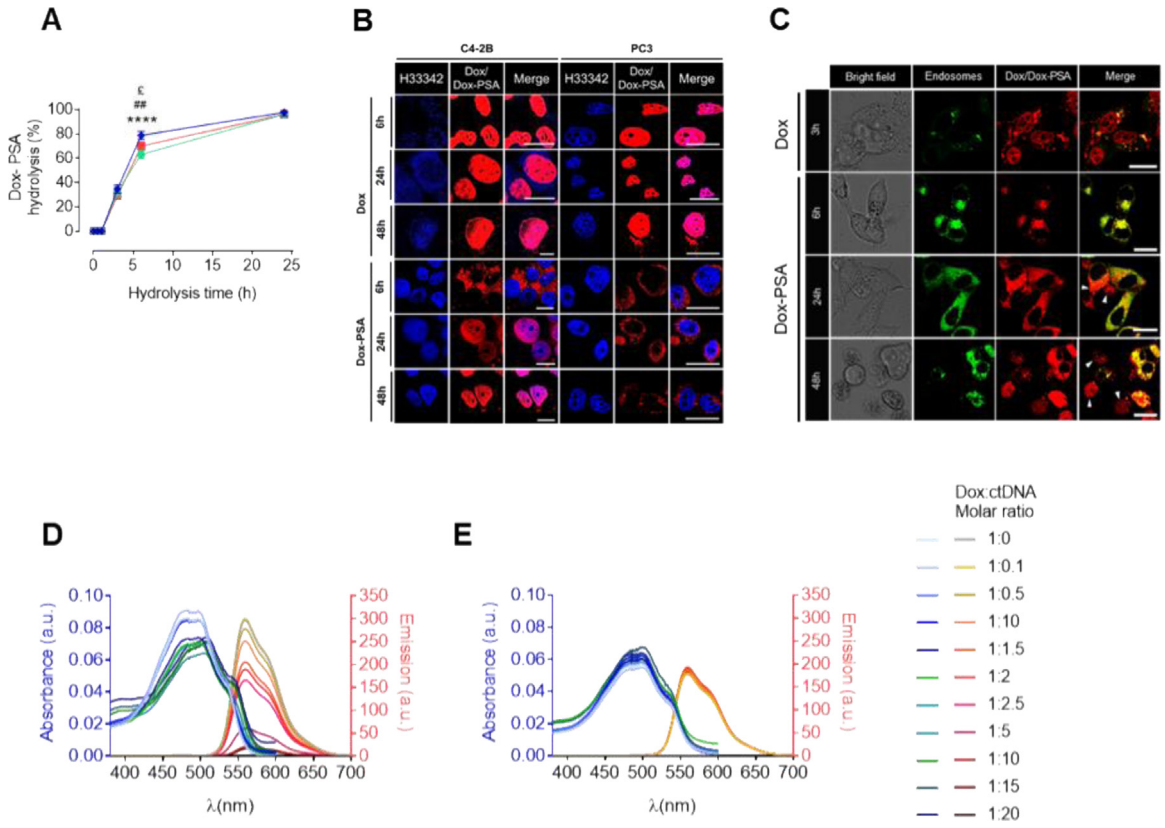

Fig. 2. Dox-PSA cleavage and selectivity. (A) Time-course of Dox-PSA cleavage as a function of the reaction temperature. The change in the area under the curve of Dox-PSA peak was monitored by a RP-HPLC equipped with a fluorescence detector (λex= 490 nm, λem= 550 nm). Data shown as mean ± SD (n = 2). Statistical significance was determined using two-way analysis of variance (ANOVA) followed by Bonferroni post-hoc test showing significant effects between room temperature (RT) and 37°C (****$p < 0.0001$), RT and 42°C (##$p < 0.01$), and 37°C and 42°C (£ $p < 0.05$), where RT, blue line; 37°C, green line and 42°C, red line. **(B)** Cellular uptake of Dox/Dox-PSA (red) in PSA-expressing (C4-2B) and non-PSA-expressing (PC3) cells as visualized by CLSM. At 24 h incubation, nuclear uptake was evident in C4-2B cells, which was not present in PC3 cells for at least 48 h of incubation. Scale bar: 20 µm. **(C)** Confocal live cell imaging of Dox and Dox-PSA (red) subcellular localization in C4-2B cells. Endosomes/lysosomes (green) were labelled with the selective Lysotracker green dye. Dox/Dox-PSA (red) co-localization with the acidic endolysosomal compartments (green) is shown in yellow. After 3 h of incubation with Dox, most of the drug was localized in the nucleus of C4-2B cells, whereas Dox-PSA signals co-localized with the endolysosomal compartments after 6 h of incubation. At 24 h, some cells showed nuclear uptake, which was accentuated at 48 h post-incubation (white arrows). Scale bar: 20 µm. Drug:DNA binding studies showing the absorbance and emission spectra of **(D)** 10 µM Dox and **(E)** Dox-PSA, as function of increasing drug:DNA molar ratio.

post-incubation (data not shown), Dox-PSA did not display any detectable nuclear uptake even after 2 h of incubation (Supporting Fig. S3). Dox is known to enter cells by passive diffusion down its concentration gradient [46,47], while most peptides cannot cross the plasma membrane through this route [48]. Therefore, we hypothesized that Dox-PSA might be internalized by the endocytic pathway. To test our hypothesis, we labeled the acidic endo/lysosomal compartments with the cell- permeable dye LysoTracker™ Green and followed the intracellular localization of Dox/Dox-PSA in C4-2B cells by CLSM. As expected, after 3 h of incubation with Dox, most of its red fluorescence was present in the nuclei, with only minor co-localization with endo/lysosomal vesicles, confirming that endocytosis plays a minor part in Dox uptake (Fig. 2**C**). Conversely, a very significant overlap between the red fluorescence from Dox-PSA and the green fluorescence from the endo/lysosomal vesicles was observed after 6 h of incubation, showing that indeed the prodrug was taken up by endocytosis. Importantly, at 24 h of incubation with Dox-PSA, some cells displayed red cytosolic fluorescent signals which did not co-localize with the green fluorescence (Fig. 2**C**), indicating that the prodrug could escape the endosomes, which is a key event for Dox-PSA to exert its downstream cytotoxic effects. In addition, nuclear uptake was observed in some cells as early as 24 h, being much more prominent with further incubation for 48 h, indicating that Dox released from Dox-PSA was present in the nuclei. To confirm that the observed nuclear fluorescence was attributed to Dox that was released from Dox-PSA, and not to Dox-PSA itself, we performed drug-DNA binding studies, which are based on the fact that Dox fluorescence is quenched when bound to DNA [29]. Thus, we titrated 10 µM of Dox (or Dox-PSA molar equivalent) with varying concentrations of calf thymus DNA (ctDNA) from 0 to 200 µM, and monitored any alterations in the absorbance and emission spectra of Dox/Dox-PSA. As anticipated, by increasing the molar ratio of Dox:ctDNA, Dox absorbance decreased, and Dox fluorescence (emission) was quenched, indicating that Dox intercalated with DNA (Fig. 2**D**). The same was not observed in the case of Dox-PSA, where the presence of ctDNA had no effect on the spectral properties of the prodrug (Fig. 2**E**). These data show that Dox-PSA does not bind to DNA and constitutes another compiling evidence for Dox-PSA prodrug selectivity. This is a fundamental aspect because, since the target of Dox cytotoxicity is the nucleus, potential Dox-PSA intercalation with DNA would setback the selectivity requirements of a prodrug approach.

3.3. Dox-PSA could be loaded and released from LTSL upon mild HT

In an attempt to improve Dox-PSA safety profile and avoid its non-specific metabolism [17], Dox-PSA was loaded into LTSL using a remote-loading method (Scheme 1), and purified using size exclusion chromatography (Supporting Fig. S4). Formulated Dox-PSA-loaded LTSL exhibited small size (~139 nm), low polydispersity index (PdI, 0.09), and slightly negative surface charge (-12 mV),

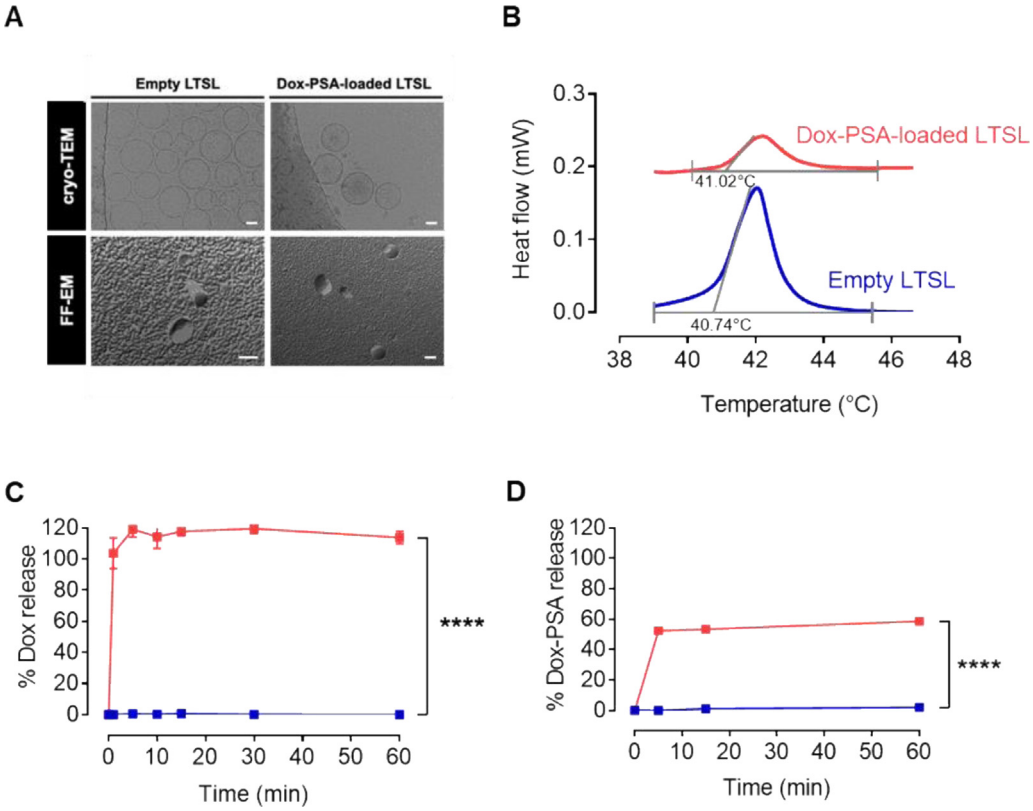

Fig. 3. Dox-PSA encapsulation and release from LTSL. (A) Representative micrographs of empty (prodrug-free) LTSL and Dox-PSA-loaded LTSL as imaged by cryo-TEM (top panel) and freeze-fracture EM (FF-EM) (bottom panel). Scale bar cryo-TEM: 50 nm, scale bar FF-EM: 100 nm **(B)** Differential scanning calorimetry (DSC) curves of empty and Dox-PSA-loaded LTSL. Calorimetric data (endothermic heat flow shown in mWatts) is shown as a function of temperature. Release profiles of **(C)** LTSL-Dox and **(D)** Dox-PSA-loaded LTSL under normothermic (37°C, blue squares) and hyperthermic (42°C, red squares) conditions. LTSL-Dox was used as a positive control for release experiments. Data shown as mean ± SD (n = 3). Statistical significance was determined using two-way analysis of variance (ANOVA) followed by Bonferroni post-hoc test showing significant results over release at 37°C (****$p < 0.0001$).

which were comparable to the empty LTSL (Supporting Table 1). Dox-PSA encapsulation efficacy (~15%) was lower than Dox (~95%, data not shown); however, it was sufficient for our *in vitro* and *in vivo* testing. Given the fact that Dox-PSA was loaded into the aqueous core of LTSL by remote loading, i.e., after liposomes were formed, we did not anticipate any alterations in the self-assembly properties of Dox-PSA-loaded-LTSL. Therefore, the morphology of Dox-PSA-loaded LTSL was studied using cryo-TEM and FF-EM. Both techniques revealed unilamellar vesicles with a spherical shape, where both the morphology and size of the prodrug-loaded LTSL were similar to those of the empty LTSL (Fig. 3**A**), in good agreement with the DLS data.

Next, differential scanning calorimetry (DSC) was used to investigate whether the encapsulation of Dox-PSA in LTSL altered the T_m. Importantly, the T_m of Dox-PSA-loaded LTSL (41.02°C) was not significantly different from that of the empty LTSL (40.74°C) (Fig. 3**B**). Furthermore, our Dox-PSA-loaded LTSL were stable at temperatures below their gel-to-liquid crystalline phase transition temperature (T_m), as shown in Supporting Fig. S5. Therefore, minimal drug release is expected below the Tm, while an efficient Dox-PSA release under mild HT (42°C) is anticipated due to lysolipid-stabilised pores formation [21,22]. LTSL-Dox which exhibit ultrafast release profile were used as a positive control in our study [21,33]. Our results showed that whilst the control LTSL-Dox released 100% of Dox within the first minute of exposure to 42°C (Fig. 3**C**), a burst release was also seen for Dox-PSA-loaded LTSL, with approximately 50% of Dox-PSA released within 5 min, however, the amount of prodrug released remained steady over the experimental time course of 60 min (Fig. 3**D**).

3.4. Mild HT triggers efficient Dox-PSA release from LTSL in C4-2B cells

In order to investigate the intracellular localization of the prodrug-loaded LTSL and to test our hypothesis that mild HT could trigger Dox-PSA release, we performed CLSM. Treated cells were either exposed to 42°C for 1 h and then returned to 37°C (42°C condition) or maintained at 37°C for the entire course of the experiment (37°C condition). Interestingly, the intrinsic fluorescence of Dox-PSA and the fact that, unlike Dox, its fluorescence was not quenched inside liposomes, allowed us to easily track the intracellular localization of free Dox-PSA or Dox-PSA-loaded LTSL in the presence or absence of mild HT. At physiological temperature (37°C), the free Dox-PSA could be detected in the nuclei of C4-2B cells at both 24 and 48 h, whilst fluorescence was confined to the cytosol when cells were treated with Dox-PSA-loaded LTSL for the same time periods (Fig. 4**A**). Remarkably, when cells were treated with Dox-PSA-loaded LTSL in combination with mild HT (42°C), Dox nuclear uptake was evident at 48 h (Fig. 4**A**). This confirms that HT triggered Dox-PSA prodrug release from these liposomes, where the released Dox-PSA was efficiently cleaved into free Dox.

3.5. Dox-PSA-loaded LTSL in combination with mild HT improvs Dox-PSA toxicity in C4-2B monolayers and spheroids

To explore whether LTSL could indeed serve as a potential delivery system for Dox-PSA, we used a resazurin assay to determine the viability of C4-2B cells treated with different concentrations of either free Dox-PSA or Dox-PSA-loaded LTSL. Strikingly, Dox-

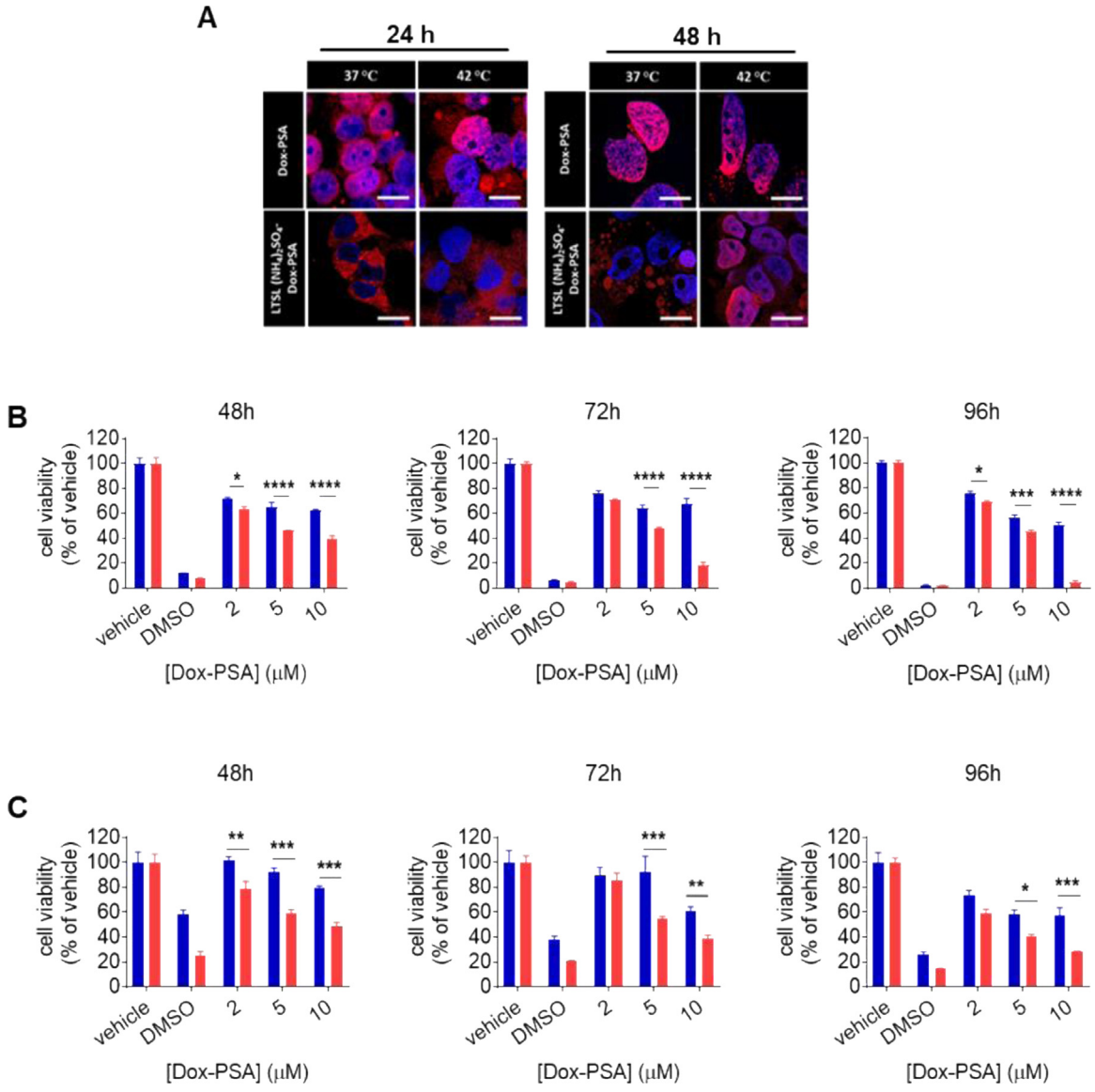

Fig. 4. Dox-PSA-loaded LTSL in combination with mild hyperthermia triggered Dox-PSA release and improved toxicity in C4-2B monolayers and spheroids. (A) Representative images showing the subcellular localization of Dox-PSA and Dox-PSA-loaded LTSL in C4-2B cells incubated at 37°C or 42°C for 1 h. The prodrug fluorescence (red) and the Hoechst 33342-stained nuclei of the cells (blue) were visualized by confocal microscopy over 24 and 48 h. Scale bar: 20 μm. **(B)** C4-2B monolayers and **(C)** spheroids were treated with increasing concentrations of Dox-PSA-loaded LTSL for 48 h (left panel), 72 h (middle panel), and 96 h (right panel). 10% (v/v) DMSO was used as a positive control for toxicity. Cells/spheroids were either incubated at 37°C for the whole course of the experiment (blue bars) or incubated at 42°C for 1 h and then returned to 37°C for the remaining time (red bars). Cell viability was quantified by resazurin assay and normalized to the vehicle-treated cells/spheroids. Data are expressed as mean ± SEM ($4 \leq n \leq 8$) for monolayers and as mean ± SEM ($n = 4$) for spheroids. Statistical significance was determined using two-way analysis of variance (ANOVA) followed by Bonferroni post-hoc test showing significant effects over cells/spheroids treated with the same prodrug concentration and not exposed to HT (*$p < 0.05$, **$p < 0.01$, ***$p < 0.001$, ****$p < 0.0001$).

PSA encapsulation in LTSL substantially reduced prodrug toxicity at 37°C, whereas exposing the cells to 42°C significantly boosted liposomal Dox-PSA toxicity in a dose-dependent fashion (Fig. 4**B**). These results show that HT efficiently triggered Dox-PSA release, in agreement with the CLSM data. The same was not observed in the case of free Dox-PSA as cell viability was comparable at 37°C and 42°C (Supporting Fig. S6A). Furthermore, to ensure that any observed toxicities were a result of prodrug release from the liposomes and not due to lipid-associated toxicities, cells were treated with empty LTSL; however no reduction in cell viability was observed (Supporting Fig. S7). To challenge the importance of Dox-PSA being released from liposomes in response to HT to induce toxicity in cells, Dox-PSA was loaded into the aqueous core of conventional liposomes [DPPC:Chol:PEG (95:50:5 molar ratio)] or into the lipid bilayer of LTSL. The lack of major toxicity (Supporting Fig. S8A) demonstrates that the conventional liposomes were too stable and that there was minimal Dox-PSA diffusion across the lipid bilayer. Similarly, when Dox-PSA was encapsulated in the bilayer of LTSL, it induced only minor toxicities at 42°C (Supporting Fig. S8B), suggesting that, when Dox-PSA was interacting with the bilayer, it was not released at the temperatures that would normally be if encapsulated into the aqueous core. These data highlight the importance of HT to trigger Dox-PSA release from LTSL to induce cytotoxicity.

The penetration of liposomes into solid tumors is a critical step for an efficient drug delivery [49]. Thus, in an attempt to evaluate the relevance of Dox-PSA-loaded LTSL to the therapy of advanced PC, we assessed the toxicity of free Dox-PSA and Dox-PSA-loaded

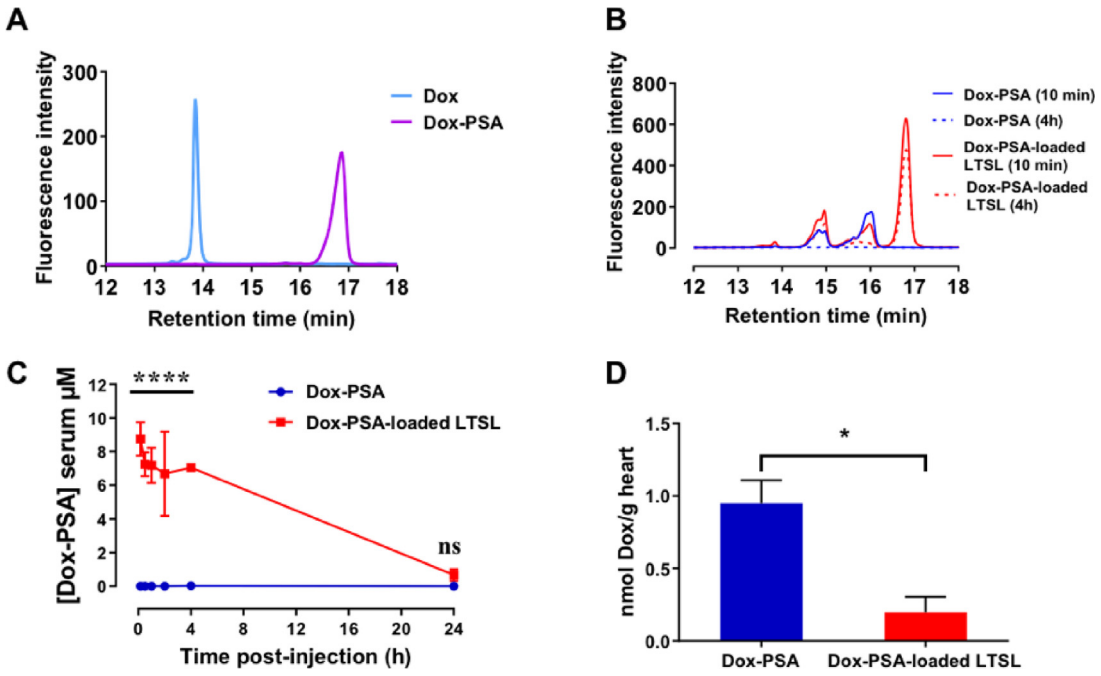

Fig. 5. Dox-PSA *in vivo* cleavage and safety. (A) HPLC chromatograms of Dox (light blue) and Dox-PSA (purple). **(B)** Serum profile of C4-2B tumor-bearing mice treated with free Dox-PSA (blue) and Dox-PSA-loaded LTSL (red). **(C)** Dox-PSA concentration in serum of C4-2B tumor-bearing mice treated with free Dox-PSA (blue) and Dox-PSA-loaded LTSL (red). Two-way ANOVA was used for statistical analysis, ****$p < 0.0001$. **(D)** quantification of Dox level (24 h) in hearts of C4-2B tumor-bearing mice treated with free Dox-PSA (blue) and Dox-PSA-loaded LTSL (red). T-test (two-tailed) was used for statistical analysis, *$p < 0.05$.

LTSL in C4-2B spheroids, which are a better model of the pathological environment [50,51]. As expected, the toxicity of free Dox-PSA was lower in spheroids compared to monolayers (Supporting Figs. S6A & S6B). In addition, mild HT did not significantly alter the toxicity profile of the free Dox-PSA (Supporting Fig. S6B). On the contrary, Dox-PSA-loaded LTSL in combination with 42°C significantly decreased spheroids viability across all the time points tested (Fig. 4**C**) to levels comparable to those achieved in 2D cultures (Fig. 4**B**). These results support our previous data where we showed that mild HT can trigger a controlled release of Dox-PSA from LTSL. Most importantly, treatment of C4-2B spheroids with Dox-PSA-loaded LTSL combined with mild HT induced a very significant reduction in the viability in contrast to the observed for the free Dox-PSA, particularly at 72 and 96 h. These encouraging results of Dox-PSA HT-triggered release can potentially be augmented *in vivo* through the increased blood flow, permeability, and extravasation of these liposomes.

3.6. Dox-PSA-loaded LTSL prolongs prodrug blood circulation and reduce heart accumulation

As the main aim of the present study was to develop a safer therapeutic approach for Dox-PSA delivery, we sought to assess the pharmacokinetics of Dox-PSA-loaded LTSL *in vivo*. Blood was collected from C4-2B tumor-bearing mice intravenously administered with either free Dox-PSA or Dox-PSA-loaded LTSL to determine their serum profile. Standard curves of Dox and Dox-PSA with a retention time of 13.8 and 16.8 min, respectively (Fig. 5**A**), were established for our quantitative analysis. For mice injected with free Dox-PSA, the fast disappearance of peak at 16.8 min happened within 10 min which indicated fast clearance/metabolism of free Dox-PSA. Furthermore, in addition to the prodrug peak, another three peaks were detected, at 14.8 min, 15.9 min, and a small peak at 13.8 min (Fig. 5**B**). The first two peaks could be attributed to the intermediate metabolites of Dox-PSA, and the last peak at 13.8 min corresponds to the final product of Dox-PSA metabolism, Dox. Moreover, at 4 h post-injection, all these peaks were reduced to undetectable levels, due to their rapid clearance. Interestingly, for mice injected with Dox-PSA-loaded LTSL, the high intensity Dox-PSA peak at 16.8 min remained for at least 4 h post-injection (Fig. 5**B**). The intermediate metabolites' peaks (14.8 and 15.9 min) and the Dox peak (13.8 min) could also be detected. Next, to determine Dox-PSA circulation time, we plotted Dox-PSA concentration in serum against the time post-injection (Fig. 5**C**). As expected, mice treated with Dox-PSA-loaded LTSL showed significantly increased Dox-PSA blood circulation compared to mice treated with free Dox-PSA, confirming that the liposomes efficiently shielded Dox-PSA from premature cleavage and activation in the bloodstream, besides reducing its systemic clearance. As Dox chemotherapy can cause dose-limiting cardiotoxicity [16], we compared Dox concentrations in the heart of mice injected with either free Dox-PSA or Dox-PSA-loaded LTSL (Fig. 5**D**). Promisingly, when the prodrug was encapsulated into LTSL, Dox accumulation in the heart was reduced by fivefold. It is worth mentioning that level of cleaved Dox in serum could not be quantified, probably due to its rapid clearance and/or tissue distribution.

3.7. Mild HT improves Dox-PSA-loaded LTSL accumulation in the tumor

To investigate Dox-PSA local accumulation in the tumor upon mild HT, C4-2B tumor-bearing mice were intravenously administered with Dox-PSA-loaded LTSL (10 mg/kg of Dox-PSA), and one of the tumor-bearing legs was immediately immersed in a 42°C water bath for 1 h (+ HT). The other tumor-bearing leg was used as a control (- HT). *In vivo* optical imaging was carried out to compare the accumulation of Dox-PSA in the solid tumor immediately after treatment termination (1 h) and 24 h post-injection. At 1 h post-injection, there was barely any Dox-PSA detected at the tumor site. However, a longer time allowed more prodrug to accumulate in both the control and heat-treated tumors (Fig. 6**A**). *In vivo* imaging of the tumors showed a slight, but not significant increase in

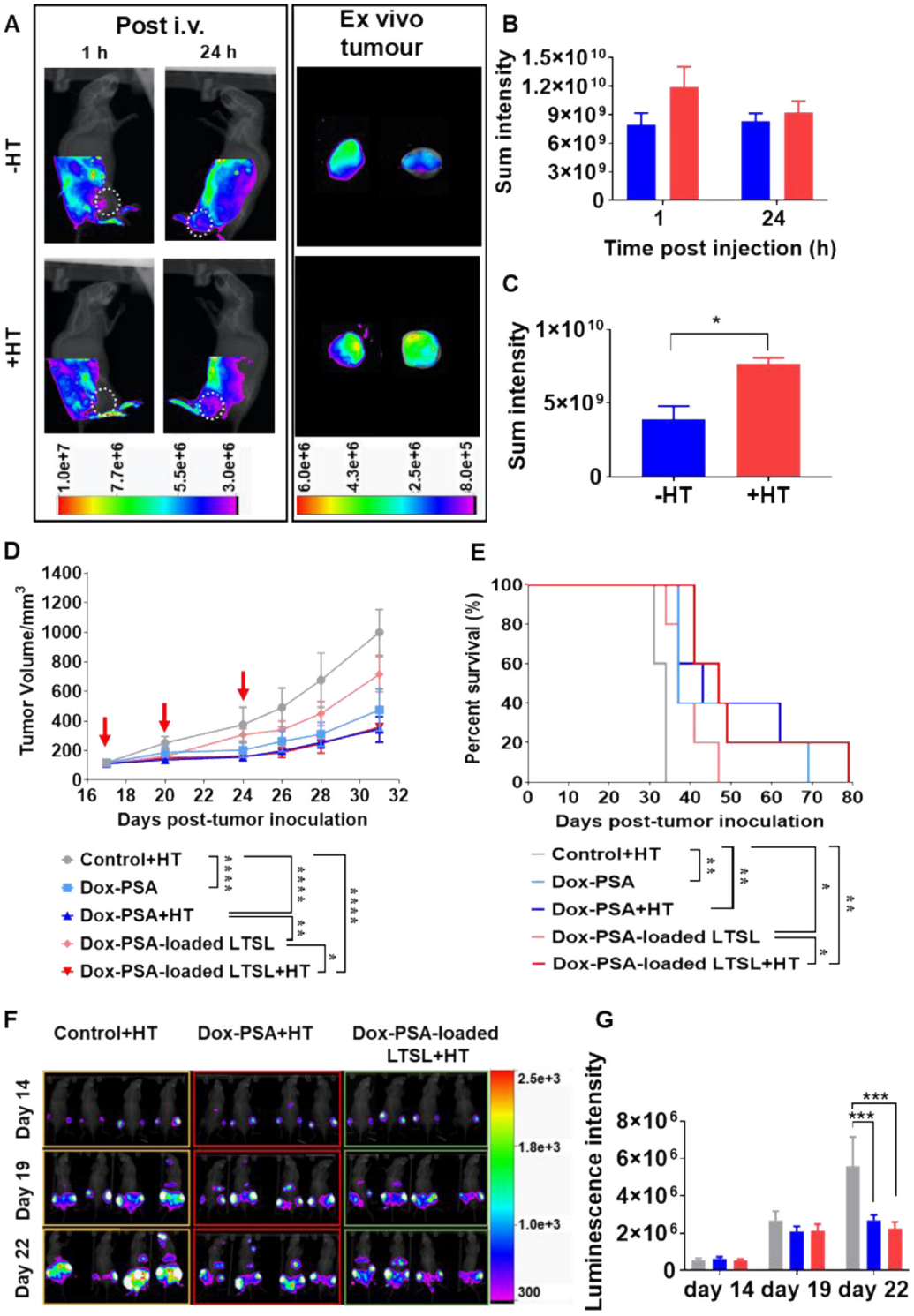

Fig. 6. ***In vivo*** **release and therapeutic efficacy of Dox-PSA-loaded LTSL in combination with mild HT. (A)** Dox-PSA-loaded LTSL release in C4-2B solid tumor in combination with mild HT. C4-2B-bearing mice were injected via the tail vein with Dox-PSA-loaded LTSL followed by 1 h HT at 42°C. *In vivo* fluorescence images taken 1 h and 24 h post-injection of Dox-PSA-loaded LTSL in the presence and absence of HT (white dotted circles indicate the position of tumors on the legs). At 24 h, tumors were isolated, and imaged *ex vivo* (λex = 480 nm, λem = 600 nm). Dox-PSA fluorescence quantification of tumors **(B)** *in vivo* and **(C)** *ex vivo*. Blue bar: treated without HT, red bar: treated with HT. Data are shown as mean ± SEM (n = 5). **(D)** Tumor growth delay graph of C4-2B solid tumor-bearing mice. Mice were treated with PBS+HT (grey dots), Dox-PSA+HT (blue up-triangles), Dox-PSA (sky blue squares), Dox-PSA-loaded LTSL+HT (red down triangles), and Dox-PSA-loaded LTSL (pink diamonds). Red arrows indicate the days of injection. Data shown as mean ± SEM (n = 5). **(E)** Percent survival curve of solid C4-2B tumor-bearing mice following treatment described in (D). PBS+HT (grey line), Dox-PSA+HT (blue line), Dox-PSA (sky blue line), Dox-PSA-loaded LTSL+HT (red line), and Dox-PSA-loaded LTSL (pink line). Data are shown as mean ± SEM (n = 5). **(F)** Bioluminescence images of the metastatic C4-2B-4 model treated with PBS, Dox-PSA or Dox-PSA-loaded LTSL in combination with 1 h HT. **(G)** Body luminescence intensity of mice treated with PBS+HT (grey bar), Dox-PSA+HT (blue bar) or Dox-PSA-loaded LTSL+HT (red bar) on day 14, 19 and 22. Data are shown as mean ± SEM (n = 5). In C4-2B-4 bone metastasis therapy experiments, mice were treated on day 14, 17, and 20 post tumor injection. In statistical analysis: $^{*}p < 0.05$, $^{**}p < 0.01$, $^{***}p < 0.001$, $^{****}p < 0.0001$.

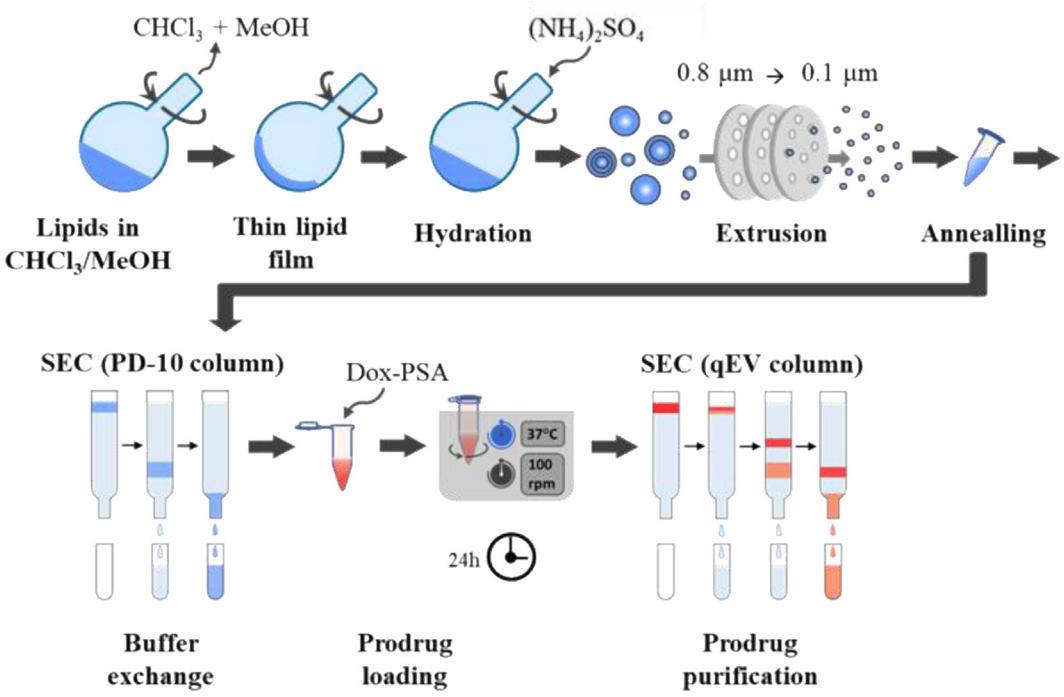

Scheme 1. Scheme illustrating the preparation of LTSL-Dox-PSA by remote loading using ammonium sulphate ($(NH_4)_2SO_4$) gradient.

Dox-PSA accumulation at 1 h in the tumor that had been exposed to 42°C compared to the control one (Fig. 6**B**), which could be justified by the combined effects of lower Dox-PSA fluorescence quantum yield (Supporting Fig. S9) and high background fluorescence from the animal. Nevertheless, *ex vivo* analysis at 24 h post-injection revealed a ~ 2-fold improvement in prodrug tumor fluorescence intensity upon mild HT treatment (Fig. 6**C**), which could be due to the following reasons: 1) more Dox-PSA-loaded LTSL accumulated in the tumor as a consequence of HT-induced increase in blood flow and liposome extravasation [52] and/or 2) Dox-PSA release and activation into Dox, with a subsequent increase in the fluorescence signal.

3.8. Dox-PSA-loaded LTSL combined with HT inhibits C4-2B xenograft growth in vivo

To assess the therapeutic efficacy of Dox-PSA-loaded LTSL in combination with HT, we carried out tumor growth retardation and survival studies. Briefly, when C4-2B tumors reached a volume of 50-100 mm^3, mice were randomized into 5 groups: PBS (control), Dox-PSA, Dox-PSA+HT, Dox-PSA-loaded LTSL and Dox-PSA-loaded LTSL+HT. Each treatment was administered via tail vein and immediately after injection, local HT treatment was applied for 1 h in the tumor-bearing leg of the mice belonging to the HT groups. Treatment schedule was administered three times with 3-4 days interval and tumor volumes were measured over 14 days from first injection. All treatments delayed tumor growth compared to control mice, except for Dox-PSA-loaded LTSL administered in the absence of HT, as tumor volumes in this group were not statistically different from tumor volumes of PBS control group. This finding indicates that Dox-PSA was not released from LTSL in the absence of HT. Excitingly, Dox-PSA-loaded LTSL combined with mild HT significantly delayed tumor growth (64% tumor volume reduction over control group at day 31), with tumors reaching comparable volumes to those in the free Dox-PSA group (Fig. 6**D**), which indicates that HT efficiently triggered Dox-PSA release from LTSL. Conversely, mild HT treatment did not improve efficacy of free Dox-PSA, as shown by similar growth retardation rates obtained with Dox-PSA with and without HT (Fig. 6**D**). Importantly, combining Dox-PSA-loaded LTSL with HT resulted in almost 3-fold reduction in tumor volume compared to the situation where Dox-PSA-loaded LTSL were administered without HT treatment (Fig. 6**D**), reinsuring that heat triggered Dox-PSA release at the tumor site . The tumor growth delay observed for the mice treated with LTSL-Dox-PSA+HT effectively extended median survival to 47 days compared to 34 days for the control mice and 43 days for the Dox-PSA+HT mice (Fig. 6**E**). Furthermore, consistent with the tumor volume data, the combined treatment of free Dox-PSA with HT did not significantly prolong survival over mice treated with free Dox-PSA (no HT). Interestingly, median survival was significantly improved from 37 days for the mice administered with Dox-PSA-loaded LTSL (no HT) to 47 days for the mice treated with a combination of Dox-PSA-loaded LTSL and mild HT (Fig. 6**E**). Furthermore, no apparent toxicity was observed in the major organs of the treated mice, compared to the control mice, as confirmed by H&E staining (Supporting Fig. S10). Finally, encouraged by the promising performance of our therapeutic strategy in a PC solid tumor model, we have also evaluated the therapeutic efficacy of Dox-PSA-loaded LTSL+HT in a C4-2B metastatic bone model. Promisingly, Dox-PSA-loaded LTSL+HT significantly delayed metastatic growth *in vivo* (Fig. 6**F** & **G**), which encourages further investigations of this combined therapy as a potential treatment for advanced oligometastatic PC.

4. Discussion

Glutaryl-Hyp-Ala-Ser-Chg-Gln-Ser-Leu-Dox (L-377,202 or Dox-PSA) is a PSA-activated prodrug that completed phase I clinical trials for metastatic PC [16,53]. However, it did not advance beyond phase I trials due to concerns with non-PSA-specific activation [17,20]. Whereas in preclinical studies with nude mice bearing LNCaP xenografts 8- to 9-fold higher doses of L-377,202 were administered in comparison to free Dox [53], the clinical scenario was largely dissimilar, where only 1.5-fold more molar equivalent of Dox could be administered. Furthermore, 1 of 6 patients treated with L-377,202 at the efficacious dose of 225 mg/m^2 exhibited dose-limiting neutropenia [54]. This undesirable cleav-

age was attributed to uncharacterized proteases. Considering recent evidence showing that PSA-alpha-2-macroglobulin (PSA-A2M) complexes present in the serum of advanced PC patients retain enzymatic activity against small peptide substrates [55], we believe that not all the serum PSA is enzymatically inactive, contrarily to what has long been a safe assumption [56,57]. Thus, the PSA-A2M complexes may also contribute to the metabolism of L-377,202 and its systemic toxicity. In efforts to improve the specificity and plasma stability of L-377,202 prodrug, Aloysius and Hu recently coupled a modified peptide sequence (GABA←mGly-Ala-Ser-Chg-Gln) to Dox using a self-immolative 3-aminooxypropionate linker to reduce non-PSA-mediated hydrolysis by human neprilysin [19,20]. The authors claimed that by optimizing the PSA-cleavable peptide promoiety and replacing the Ser-Leu linker with a 3-aminooxypropionate linker, non-PSA-mediated hydrolysis by human neprilysin, which they hypothesize could contribute to L-377,202 instability *in vivo*, could be mitigated [19]. Furthermore, it was determined that whilst substitutions between P1 and P4 would adversely impact PSA specificity, the given modifications at P5 enhanced PSA-mediated cleavage rate and decreased non-PSA-specific hydrolysis [19,20].

In light of these results, new and versatile strategies are needed to accelerate the clinical translational of Dox-PSA and other promising PSA-activatable prodrugs of 5-fluorodeoxyuridine, vinblastine, thapsigargin, paclitaxel, LY294002, and glycophosphatidylinositol [53,58-60]. In the current research, we focused on developing a therapeutic approach that could 1) overcome the caveat of non-specific Dox-PSA cleavage, 2) finely tune prodrug activation and 3) provide a safer option for Dox-PSA administration, particularly for the treatment of patients with high-risk localized PC, which currently have a poor prognosis. To fulfil these objectives, we encapsulated Dox-PSA into clinically relevant LTSL to finely tune the physicochemical properties of the prodrug without any chemical modifications.

To date, a range of prodrugs has been loaded into nanocarriers to boost their efficacy and/or safety [61,62]. For instance, several articles have been published reporting acid-responsive polymeric Dox prodrug nanoparticles for chemotherapy or combined photothermal-chemotherapy to treat cancer [63–65]. These Dox prodrug-loaded nanoparticles were synthesized by introducing an acid-labile bond, enabling its activation in the acidic tumour environment. However, this approach cannot exclude the possibility of prodrug activation in the endosomes of healthy cells. To enhance selectivity to cancer cells, cathepsin B-cleavable Dox prodrugs have been synthesized. More interestingly, several cathepsin B-cleavable Dox- HPMA copolymers have been developed to prolong the prodrug blood circulation [66]. Recently, Yang *et. al.* engineered cathepsin B-cleavable Dox prodrug nanoparticle [67]. The prodrug was chemically conjugated to a cathepsin B-cleavable peptide that successfully self-assembled into nanoparticles stabilized with pluronic F68. Interestingly, these engineered nanoparticles induced immunogenic cell death against the targeted cancer cells and potentiated PD-L1 checkpoint inhibitor immunotherapy. These findings collectively highlight the potential benefits of prodrugs loading into nanoparticles.

To the best of our knowledge, there are no published reports of remote loading of Dox-PSA prodrugs into nanocarriers. So far, our group has loaded Dox-PSA into liposomes [21] and biomimetic nanovesicles [37]. In our first study, pH-sensitive liposomes were used as a model membrane to block Dox-PSA activation extracellularly, thus proving the possibility of intracellular Dox-PSA activation using in 2D and 3D *in vitro* models [21]. More recently, we encapsulated Dox-PSA into PSMA-targeted biomimetic nanovesicles as dually targeted nanoparticles to treat advanced PC [37]. However, we observed that loading Dox-PSA into non-targeted nanovesicles, unlike the PSMA-targeted ones, reduced the prodrug therapeutic efficacy *in vivo*, emphasizing the importance of efficient prodrug release. The novelty of the current research relies on loading Dox-PSA prodrug, into thermosensitive liposomes to control its release without jeopardizing its efficacy *in vivo* (Fig. 6). Interestingly, our unprecedented HT results revealed that a mild HT (42°C) treatment regimen of 1 h did not have a negative impact on either the PSA levels (Fig. 1**C**), PC cell viability (Fig. 1**D**) or PSA-mediated prodrug activation (Fig. 2**A**), which is a crucial finding to explore treatment protocols that combine Dox-PSA (or other PSA-activated prodrugs) cytotoxicity with HT treatment. Moreover, combining LTSL with mild HT provides spatial and temporal control over Dox-PSA release, which only occurs upon exposure to temperatures higher than the liposomes T_m and therefore offers a tight control over prodrug activation [68] (Fig. 4). The formulated Dox-PSA-loaded LTSL displayed a favorable size and maintained a phase transition temperature compatible with heat-triggered prodrug release. Unexpectedly, mild HT treatment for 60 min released only 50% of Dox-PSA from LTSL, unlike Dox, where burst and complete release was obtained under similar conditions (Fig. 3) [22]. In support of our findings, few studies have shown an incomplete release of macromolecules from LTSL, in which ~ 46% of a 4 kDa dextran, ~ 40% of FITC-albumin, and ~ 70% of FITC-lysozyme were released after 30 min of incubation at 42°C [69,70]. The reason behind the incomplete Dox-PSA release from LTSL remains elusive, but it could be due to the fact that Dox-PSA is a considerably larger molecule compared to Dox and due to the presence of the peptide, which confers some degree of hydrophobicity. These factors could result in some prodrug molecules obstructing some of the nanopores at the grain boundary regions in the melting bilayer and blocking/delaying further release [21]. Moreover, as these studies were carried out in a simple physiological buffer, we anticipate that higher Dox-PSA release will be achieved *in vitro* and *in vivo* where liposomes interact with different cellular components. Promisingly, despite the lower release profile in PBS, Dox-PSA-loaded LTSL in combination with mild HT were more cytotoxic than the free Dox-PSA in both PC monolayers and spheroids (Fig. 4). This is likely due to the orchestrated actions that result from the increased cellular uptake at 42°C, enhanced Dox-PSA prodrug solubility when encapsulated into LTSL and synergistic effects with HT treatment [25].

To date, this is the first published report that thoroughly investigated Dox-PSA selectivity towards PSA-expressing cells. Previously, we reported the higher selectivity of Dox-PSA to C4-2B cells (PSA+) versus PC3 cells (PSA-) by comparing the IC_{50} values of the prodrug in both cell lines [21,53]. Dox-PSA *in vitro* selectivity was further confirmed using confocal microscopy and drug-DNA binding studies (Fig. 2). Despite the high Dox-PSA selectivity *in vitro*, it still suffers from non-specific cleavage *in vivo* (Fig. 5). Dox-PSA cleavage has been reported in a few studies using PC cell/tumor lysates, human plasma or enzymatically active PSA from human seminal fluid [17,19,53]. However, no one has studied Dox-PSA *in vivo* cleavage in C4-2B solid tumor-bearing mice, as a model of CRPC, following intravenous administration. Herein, our results (Fig. 5) showed quick elimination of Dox-PSA from the blood of C4-2B tumor-bearing mice, which could be attributed to the prodrug cleavage and conversion into Dox and other intermediate metabolites that were cleared from blood circulation by various organs. However, mice injected with Dox-PSA-loaded LTSL showed significantly higher Dox-PSA concentrations in the blood, where a high fraction of Dox-PSA remained unmetabolized after 4 h compared to mice injected with free Dox-PSA (undetectable 10 min post-injection). These exciting results showed that Dox-PSA was efficiently protected from premature cleavage and clearance from blood following loading into LTSL. This extended blood circulation does not only grant more time for the prodrug to accumulate at the tumor site (where it should be activated), but also reduces its

cardiotoxicity by preventing Dox-PSA systemic activation. In support of this, Dox accumulation in the heart tissue (main site of Dox toxicity) was reduced by ~80% when Dox-PSA was encapsulated into LTSL, showing that this therapeutic strategy greatly improved the safety profile of Dox-PSA. More importantly, using the current therapy regimen, Dox-PSA-loaded LTSL combined with HT significantly delayed tumor growth at a similar rate as mice treated with free Dox-PSA in both solid and metastatic PC tumor models (Fig. 6). This indicates that our thermosensitive LTSL could block the systemic cleavage of Dox-PSA without reducing its efficacy *in vivo*. However, future studies could be conducted using higher and/or more frequent dosing regimens to boost Dox-PSA-loaded LTSL therapeutic efficacy *in vivo*.

5. Conclusion

Encapsulating Dox-PSA into clinically-relevant LTSL might represent a safer approach over administration of free Dox-PSA as it provides tight control over Dox-PSA release and activation, thus mitigating non-specific prodrug cleavage and reducing the accumulation of Dox in the heart. More importantly, Dox-PSA-loaded LTSL combined with mild HT are expected to increase the therapeutic window of Dox-PSA, where higher doses can potentially be administered without unwanted side effects.

Funding sources

This work was supported by the Prostate Cancer UK (Grant CDF12-002), the Engineering and Physical Sciences Research Council (EPSRC) (EP/M008657/1), The Royal Society (RG2014 R1), University of East Anglia and Queen's University Belfast.

Declaration of Competing Interest

The authors declare that they have no known competing financial interests or personal relationships that could have appeared to influence the work reported in this paper.

Acknowledgment

Authors would like to acknowledge Dr Calvin C. L. Cheung (School of Pharmacy, Queen's University Belfast) for his help with the DSC studies, and Dr Marc C. A. Stuart (Electron Microscopy, University of Groningen, The Netherlands) for cryo-EM imaging.

Supplementary materials

Viability of C4-2B cells after treatment with Dox or Dox-PSA and different mild HT regimens (Supporting Fig. S1), AMC-PSA hydrolysis by enzymatically active PSA (Supporting Fig. S2), Subcellular localization of Dox-PSA in PC cells (Supporting Fig. S3), Purification of Dox-PSA-loaded LTSL by size exclusion chromatography (SEC) (Supporting Fig. S4), Physicochemical characterization of Dox-PSA-loaded LTSL (Table S1), Effect of temperature on LTSL stability (Supporting Fig. S5), Viability of C4-2B models after treatment with free Dox-PSA ± HT (Supporting Fig. 6S), Viability of C4-2B cells after treatment with empty (prodrug-free) LTSL (Supporting Fig. S7), Viability of C4-2B cells after treatment with DPPC:Chol:DSPE-PEG_{2000} and bilayer-loaded LTSL (Fig. S9), Fluorescence properties of Dox-PSA (Fig. S9), H&E staining (Supporting Fig. S10), and changes in mice body weight (Supporting Fig. S11).

Supplementary material associated with this article can be found, in the online version, at doi:10.1016/j.actbio.2021.12.019.

References

[1] F. Bray, J. Ferlay, I. Soerjomataram, R.L. Siegel, L.A. Torre, A. Jemal, Global cancer statistics 2018: GLOBOCAN estimates of incidence and mortality worldwide for 36 cancers in 185 countries, CA Cancer J. Clin. 68 (6) (2018) 394–424.
[2] M.S. Litwin, H.-J. Tan, The diagnosis and treatment of prostate cancer, JAMA 317 (24) (2017) 2532.
[3] E. Francini, M.-E. Taplin, Prostate cancer: developing novel approaches to castration-sensitive disease, Cancer 123 (1) (2017) 29–42.
[4] S. Ramalingam, V.P. Ramamurthy, V.C.O. Njar, Dissecting major signaling pathways in prostate cancer development and progression: mechanisms and novel therapeutic targets, J. Steroid Biochem. Mol. Biol. 166 (2017) 16–27.
[5] M. Pagliuca, C. Buonerba, K. Fizazi, G. Di Lorenzo, The evolving systemic treatment landscape for patients with advanced prostate cancer, Drugs 79 (4) (2019) 381–400.
[6] S. Sumanasuriya, J. De Bono, Treatment of advanced prostate cancer—a review of current therapies and future promise, Cold Spring Harb. Perspect. Med. 8 (6) (2018) a030635.
[7] A. Sharp, I. Coleman, W. Yuan, C. Sprenger, D. Dolling, D.N. Rodrigues, J.W. Russo, I. Figueiredo, C. Bertan, G. Seed, R. Riisnaes, T. Uo, A. Neeb, J. Welti, C. Morrissey, S. Carreira, J. Luo, P.S. Nelson, S.P. Balk, L.D. True, J.S. De Bono, S.R. Plymate, Androgen receptor splice variant-7 expression emerges with castration resistance in prostate cancer, J. Clin. Invest. 129 (1) (2018) 192–208.
[8] L. Dong, R.C. Zieren, W. Xue, T.M. De Reijke, K.J. Pienta, Metastatic prostate cancer remains incurable, why? Asian J. Urol. 6 (1) (2019) 26–41.
[9] P.A. Watson, V.K. Arora, C.L. Sawyers, Emerging mechanisms of resistance to androgen receptor inhibitors in prostate cancer, Nat. Rev. Cancer 15 (12) (2015) 701–711.
[10] A. Najjar, R. Karaman, The prodrug approach in the era of drug design, Expert Opin. Drug Deliv. 16 (1) (2019) 1–5.
[11] J.S. Dudani, A.D. Warren, S.N. Bhatia, Harnessing protease activity to improve cancer care, Ann. Rev. Cancer Biol. 2 (1) (2018) 353–376.
[12] K. Hannu, M. Johanna, S. Ulf-Håkan, KLK-targeted therapies for prostate cancer, EJIFCC 25 (2) (2014) 207–218.
[13] M. Elhilali Mostafa, P. Pommerville, C. Yocum Richard, R. Merchant, G. Roehrborn Claus, R. Denmeade Samuel, Prospective, randomized, double-blind, vehicle controlled, multicenter phase IIb clinical trial of the pore forming protein PRX302 for targeted treatment of symptomatic benign prostatic hyperplasia, J. Urol. 189 (4) (2013) 1421–1426.
[14] Sophiris bio provides updates on phase 2b localized prostate cancer trial, https://www.prnewswire.com/news-releases/sophiris-bio-provides-updates-on-phase-2b-localized-prostate-cancer-trial-300767234.html 2018 (Accessed 26 August 2021).
[15] Sophiris bio receives positive feedback from FDA regarding phase 3 localized prostate cancer clinical trial design, https://www.prnewswire.com/news-releases/sophiris-bio-receives-positive-feedback-from-fda-regarding-phase-3-localized-prostate-cancer-clinical-trial-design-300941740.html 2019 (Accessed 26 August 2021).
[16] V.M. Garsky, P.K. Lumma, D.-M. Feng, J. Wai, H.G. Ramjit, M.K. Sardana, A. Oliff, R.E. Jones, D. Defeo-Jones, R.M. Freidinger, The synthesis of a prodrug of doxorubicin designed to provide reduced systemic toxicity and greater target efficacy, J. Med. Chem. 44 (24) (2001) 4216–4224.
[17] B.K. Wong, D. DeFeo-Jones, R.E. Jones, V.M. Garsky, D.-M. Feng, A. Oliff, M. Chiba, J.D. Ellis, J.H. Lin, PSA-specific and non-PSA-specific conversion of a PSA-targeted peptide conjugate of doxorubicin to its active metabolites, Drug Metab. Dispos. 29 (3) (2001) 313.
[18] H. Aloysius, L. Hu, Targeted prodrug approaches for hormone refractory prostate cancer, Med. Res. Rev. 35 (3) (2015) 554–585.
[19] H. Aloysius, L. Hu, Synthesis and evaluation of new peptide-linked doxorubicin conjugates as prodrugs activated by prostate-specific antigen, Med. Chem. Res. 29 (7) (2020) 1280–1299.
[20] H. Aloysius, L. Hu, Improving the specificity of the prostate-specific antigen substrate Glutaryl-Hyp-Ala-Ser-Chg-Gln as a promoiety, Chem. Biol. Drug Des. 86 (4) (2015) 837–848.
[21] D. Needham, J.-Y. Park, A.M. Wright, J. Tong, Materials characterization of the low temperature sensitive liposome (LTSL): effects of the lipid composition (lysolipid and DSPE–PEG2000) on the thermal transition and release of doxorubicin, Faraday Discuss 161 (0) (2013) 515–534.
[22] W.T. Al-Jamal, Z.S. Al-Ahmady, K. Kostarelos, Pharmacokinetics & tissue distribution of temperature-sensitive liposomal doxorubicin in tumor-bearing mice triggered with mild hyperthermia, Biomaterials 33 (18) (2012) 4608–4617.
[23] B. Hildebrandt, P. Wust, O. Ahlers, A. Dieing, G. Sreenivasa, T. Kerner, R. Felix, H. Riess, The cellular and molecular basis of hyperthermia, Crit. Rev. Oncol. Hematol. 43 (1) (2002) 33–56.
[24] A.G. Van Der Heijden, M.W. Dewhirst, Effects of hyperthermia in neutralising mechanisms of drug resistance in non-muscle-invasive bladder cancer, Int. J. Hyperthermia 32 (4) (2016) 434–445.
[25] P. Wust, B. Hildebrandt, G. Sreenivasa, B. Rau, J. Gellermann, H. Riess, R. Felix, P.M. Schlag, Hyperthermia in combined treatment of cancer, Lancet Oncol. 3 (8) (2002) 487–497.
[26] Z. Vujaskovic, D.W. Kim, E. Jones, L. Lan, L. McCall, M.W. Dewhirst, O. Craciunescu, P. Stauffer, V. Liotcheva, A. Betof, K. Blackwell, A phase I/II study of neoadjuvant liposomal doxorubicin, paclitaxel, and hyperthermia in locally advanced breast cancer, Int. J. Hyperthermia 26 (5) (2010) 514–521.

[27] R.J. Griffin, R.P.M. Dings, A. Jamshidi-Parsian, C.W. Song, Mild temperature hyperthermia and radiation therapy: role of tumour vascular thermotolerance and relevant physiological factors, Int. J. Hyperthermia 26 (3) (2010) 256–263.
[28] S.G.T. Pereira, S. Hudoklin, M.E. Kreft, N. Kostevsek, M.C.A. Stuart, W.T. Al-Jamal, Intracellular activation of a prostate specific antigen-cleavable doxorubicin prodrug: a key feature toward prodrug-nanomedicine design, Mol. Pharmaceut. 16 (4) (2019) 1573–1585.
[29] A. Di Marco, A.M. Casazza, R. Gambetta, R. Supino, F. Zunino, Relationship between activity and amino sugar stereochemistry of daunorubicin and adriamycin derivatives, Cancer Res. 36 (6) (1976) 1962–1966.
[30] A. Ruiz, G. Ma, J. Seitsonen, S.G.T. Pereira, J. Ruokolainen, W.T. Al-Jamal, Encapsulated doxorubicin crystals influence lysolipid temperature-sensitive liposomes release and therapeutic efficacy in vitro and in vivo, J. Control Release 328 (2020) 665–678.
[31] C.C.L. Cheung, G. Ma, K. Karatasos, J. Seitsonen, J. Ruokolainen, C.R. Koffi, H. Hassan, W.T. Al-Jamal, Liposome-templated indocyanine Green J- aggregates for in vivo near-infrared imaging and stable photothermal heating, Nanotheranostics 4 (2) (2020) 91–106.
[32] G. Ma, N. Kostevsek, I. Monaco, A. Ruiz, B. Markelc, C.C.L. Cheung, S. Hudoklin, M.E. Kreft, H. Hassan, M. Barker, J. Conyard, C. Hall, S. Meech, A.G. Mayes, I. Sersa, M. Cemazar, K. Markovic, J. Scancar, M.C. Franchini, W.T. Al-Jamal, PD1 blockade potentiates the therapeutic efficacy of photothermally-activated and MRI-guided low temperature-sensitive magnetoliposomes, J. Control Release (2021).
[33] J.-Y. P, Chelsea D. Landon, David Needham, Mark W. Dewhirst, Nanoscale drug delivery and hyperthermia : the materials design and preclinical and clinical testing of low temperature-sensitive liposomes used in combination with mild hyperthermia in the treatment of local cancer, Open Nanomed. J. 3 (2011) 38–64.
[34] M. Chiu, E. Prenner, Differential scanning calorimetry: an invaluable tool for a detailed thermodynamic characterization of macromolecules and their interactions, J. Pharm. Bioallied Sci. 3 (1) (2011) 39–59.
[35] T.D. Schmittgen, K.J. Livak, Analyzing real-time PCR data by the comparative CT method, Nat. Protoc. 3 (6) (2008) 1101–1108.
[36] A. Single, H. Beetham, B.J. Telford, P. Guilford, A. Chen, A comparison of real-time and endpoint cell viability assays for improved synthetic lethal drug validation, J. Biomol. Screen 20 (10) (2015) 1286–1293.
[37] G. Ma, M. Severic, M. Barker, S. Pereira, A. Ruiz, C.C.L. Cheung, W.T. Al-Jamal, Dually targeted bioinspired nanovesicle delays advanced prostate cancer tumour growth in vivo, Acta Biomater. (2021).
[38] M. Severic, G. Ma, S.G.T. Pereira, A. Ruiz, C.C.L. Cheung, W.T. Al-Jamal, Genetically-engineered anti-PSMA exosome mimetics targeting advanced prostate cancer in vitro and in vivo, J. Control Release 330 (2020) 101–110.
[39] P. Saxena, M. Trerotola, T. Wang, J. Li, A. Sayeed, J. VanOudenhove, D.S. Adams, T.J. FitzGerald, D.C. Altieri, L.R. Languino, PSA regulates androgen receptor expression in prostate cancer cells, Prostate 72 (7) (2012) 769–776.
[40] T. Matsuoka, K. Shigemura, F. Yamamichi, M. Fujisawa, M. Kawabata, T. Shirakawa, Detection of tumor markers in prostate cancer and comparison of sensitivity between real time and nested PCR, Kobe J. Med. Sci. 58 (2) (2012) E51–E59.
[41] O.S. Nielsen, J. Overgaard, Importance of preheating temperature and time for the induction of thermotolerance in a solid tumour in vivo, Br. J. Cancer 46 (6) (1982) 894–903.
[42] J.L. Roti Roti, Cellular responses to hyperthermia (40–46°C): cell killing and molecular events, Int. J. Hyperthermia 24 (1) (2008) 3–15.
[43] A. Kariya, Y. Tabuchi, T. Yunoki, T. Kondo, Identification of common gene networks responsive to mild hyperthermia in human cancer cells, Int. J. Mol. Med. 32 (1) (2013) 195–202.
[44] Q. Song, X. Chuan, B. Chen, B. He, H. Zhang, W. Dai, X. Wang, Q. Zhang, A smart tumor targeting peptide–drug conjugate, pHLIP-SS-DOX: synthesis and cellular uptake on MCF-7 and MCF-7/Adr cells, Drug Deliv. (2015) 1–13.
[45] H. Guan, M.J. McGuire, S. Li, K.C. Brown, Peptide-targeted polyglutamic acid doxorubicin conjugates for the treatment of $\alpha v\beta 6$-positive cancers, Bioconjugate Chem. 19 (9) (2008) 1813–1821.
[46] O. Tacar, P. Sriamornsak, C.R. Dass, Doxorubicin: an update on anticancer molecular action, toxicity and novel drug delivery systems, J. Pharm. Pharmacol. 65 (2) (2012) 157–170.
[47] T.M. Allen, P.R. Cullis, Liposomal drug delivery systems: from concept to clinical applications, Adv. Drug Delivery Rev. 65 (1) (2013) 36–48.
[48] N.J. Yang, M.J. Hinner, Getting across the cell membrane: an overview for small molecules, peptides, and proteins, in: A. Gautier, M.J. Hinner (Eds.), Site-Specific Protein Labeling: Methods and Protocols, Springer New York, New York, NY, 2015, pp. 29–53.
[49] L. Kou, Q. Yao, S. Sivaprakasam, Q. Luo, Y. Sun, Q. Fu, Z. He, J. Sun, V. Ganapathy, Dual targeting of l-carnitine-conjugated nanoparticles to OCTN2 and ATB0,+ to deliver chemotherapeutic agents for colon cancer therapy, Drug Deliv. 24 (1) (2017) 1338–1349.
[50] F. Mittler, P. Obeïd, A.V. Rulina, V. Haguet, X. Gidrol, M.Y. Balakirev, High-content monitoring of drug effects in a 3D spheroid model, Front. Oncol. 7 (293) (2017).
[51] E.O. Mosaad, K.F. Chambers, K. Futrega, J.A. Clements, M.R. Doran, The Microwell-mesh: a high-throughput 3D prostate cancer spheroid and drug-testing platform, Sci. Rep. 8 (1) (2018).
[52] L. Li, T.L.M. ten Hagen, M. Bolkestein, A. Gasselhuber, J. Yatvin, G.C. van Rhoon, A.M.M. Eggermont, D. Haemmerich, G.A. Koning, Improved intratumoral nanoparticle extravasation and penetration by mild hyperthermia, J. Controlled Release 167 (2) (2013) 130–137.
[53] D. DeFeo-Jones, V.M. Garsky, B.K. Wong, D.-M. Feng, T. Bolyar, K. Haskell, D.M. Kiefer, K. Leander, E. McAvoy, P. Lumma, J. Wai, E.T. Senderak, S.L. Motzel, K. Keenan, M.V. Zwieten, J.H. Lin, R. Freidinger, J. Huff, A. Oliff, R.E. Jones, A peptide–doxorubicin 'prodrug' activated by prostate-specific antigen selectively kills prostate tumor cells positive for prostate-specific antigen in vivo, Nat. Med. 6 (11) (2000) 1248–1252.
[54] R.S. DiPaola, J. Rinehart, J. Nemunaitis, S. Ebbinghaus, E. Rubin, T. Capanna, M. Ciardella, S. Doyle-Lindrud, S. Goodwin, M. Fontaine, N. Adams, A. Williams, M. Schwartz, G. Winchell, K. Wickersham, P. Deutsch, S.-L. Yao, Characterization of a novel prostate-specific antigen–activated peptide-doxorubicin conjugate in patients with prostate cancer, J. Clin. Oncol. 20 (7) (2002) 1874–1879.
[55] M.B. Kostova, W.N. Brennen, D. Lopez, L. Anthony, H. Wang, E. Platz, S.R. Denmeade, PSA-alpha-2-macroglobulin complex is enzymatically active in the serum of patients with advanced prostate cancer and can degrade circulating peptide hormones, Prostate 78 (11) (2018) 819–829.
[56] H. Lilja, D. Ulmert, A.J. Vickers, Prostate-specific antigen and prostate cancer: prediction, detection and monitoring, Nat. Rev. Cancer 8 (4) (2008) 268–278.
[57] A.M. LeBeau, M. Kostova, C.S. Craik, S.R. Denmeade, Prostate-specific antigen: an overlooked candidate for the targeted treatment and selective imaging of prostate cancer, 391(4) (2010) 333-343.
[58] D. Baiz, T.A. Pinder, S. Hassan, Y. Karpova, F. Salsbury, M.E. Welker, G. Kulik, Synthesis and characterization of a novel prostate cancer-targeted phosphatidylinositol-3-kinase inhibitor prodrug, J. Med. Chem. 55 (18) (2012) 8038–8046.
[59] S.F. Brady, J.M. Pawluczyk, P.K. Lumma, D.-M. Feng, J.M. Wai, R. Jones, D. DeFeo-Jones, B.K. Wong, C. Miller-Stein, J.H. Lin, A. Oliff, R.M. Freidinger, V.M. Garsky, Design and synthesis of a pro-drug of vinblastine targeted at treatment of prostate cancer with enhanced efficacy and reduced systemic toxicity, J. Med. Chem. 45 (21) (2002) 4706–4715.
[60] S.R. Denmeade, C.M. Jakobsen, S. Janssen, S.R. Khan, E.S. Garrett, H. Lilja, S.B. Christensen, J.T. Isaacs, Prostate-specific antigen-activated thapsigargin prodrug as targeted therapy for prostate cancer, J. Natl. Cancer Inst. 95 (13) (2003) 990–1000.
[61] M. Sancho-Albero, B. Rubio-Ruiz, A.M. Pérez-López, V. Sebastián, P. Martín–Duque, M. Arruebo, J. Santamaría, A. Unciti-Broceta, Cancer-derived exosomes loaded with ultrathin palladium nanosheets for targeted bioorthogonal catalysis, Nat. Catal. 2 (10) (2019) 864–872.
[62] U. Altanerova, J. Jakubechova, K. Benejova, P. Priscakova, V. Repiska, A. Babelova, B. Smolkova, C. Altaner, Intracellular prodrug gene therapy for cancer mediated by tumor cell suicide gene exosomes, Int. J. Cancer 148 (1) (2021) 128–139.
[63] J. Song, B. Xu, H. Yao, X. Lu, Y. Tan, B. Wang, X. Wang, Z. Yang, Schiff-linked PEGylated doxorubicin prodrug forming ph-responsive nanoparticles with high drug loading and effective anticancer therapy, Front. Oncol. 11 (890) (2021).
[64] Y. Zhang, C. Teh, M. Li, C.Y. Ang, S.Y. Tan, Q. Qu, V. Korzh, Y. Zhao, Acid-responsive polymeric doxorubicin prodrug nanoparticles encapsulating a near-infrared dye for combined photothermal-chemotherapy, Chem. Mater. 28 (19) (2016) 7039–7050.
[65] P. Gou, W. Liu, W. Mao, J. Tang, Y. Shen, M. Sui, Self-assembling doxorubicin prodrug forming nanoparticles for cancer chemotherapy: synthesis and anticancer study in vitro and in vivo, J. Mater. Chem. B 1 (3) (2013) 284–292.
[66] Y.-J. Zhong, L.-H. Shao, Y. Li, Cathepsin B-cleavable doxorubicin prodrugs for targeted cancer therapy, Int. J. Oncol. 42 (2) (2013) 373–383.
[67] S. Yang, M.K. Shim, W.J. Kim, J. Choi, G.-H. Nam, J. Kim, J. Kim, Y. Moon, H.Y. Kim, J. Park, Y. Park, I.-S. Kim, J.H. Ryu, K. Kim, Cancer-activated doxorubicin prodrug nanoparticles induce preferential immune response with minimal doxorubicin-related toxicity, Biomaterials 272 (2021) 120791.
[68] G.A. Koning, A.M.M. Eggermont, L.H. Lindner, T.L.M. ten Hagen, Hyperthermia and thermosensitive liposomes for improved delivery of chemotherapeutic drugs to solid tumors, Pharm. Res. 27 (8) (2010) 1750–1754.
[69] X. Huang, M. Li, R. Bruni, P. Messa, F. Cellesi, The effect of thermosensitive liposomal formulations on loading and release of high molecular weight biomolecules, Int. J. Pharm. 524 (1) (2017) 279–289.
[70] M.B.C. de Matos, N. Beztsinna, C. Heyder, M.H.A.M. Fens, E. Mastrobattista, R.M. Schiffelers, G. Leneweit, R.J. Kok, Thermosensitive liposomes for triggered release of cytotoxic proteins, Eur. J. Pharm. Biopharm. 132 (2018) 211–221.